



# Massive formation of lawsonite in subducted sediments from the Schistes Lustrés (W. Alps): Implications for mass transfer and decarbonation in cold subduction zones

Benjamin Lefeuvre, Philippe Agard, Anne Verlaquet, Benoît Dubacq, Alexis Plunder

## ► To cite this version:

Benjamin Lefeuvre, Philippe Agard, Anne Verlaquet, Benoît Dubacq, Alexis Plunder. Massive formation of lawsonite in subducted sediments from the Schistes Lustrés (W. Alps): Implications for mass transfer and decarbonation in cold subduction zones. *Lithos*, 2020, 10.1016/j.lithos.2020.105629 . hal-02886116

**HAL Id: hal-02886116**

**<https://brgm.hal.science/hal-02886116>**

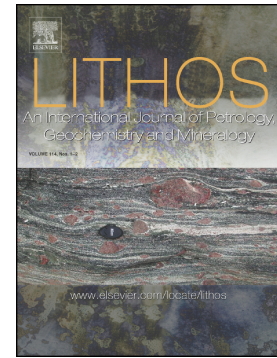
Submitted on 8 Jul 2020

**HAL** is a multi-disciplinary open access archive for the deposit and dissemination of scientific research documents, whether they are published or not. The documents may come from teaching and research institutions in France or abroad, or from public or private research centers.

L'archive ouverte pluridisciplinaire **HAL**, est destinée au dépôt et à la diffusion de documents scientifiques de niveau recherche, publiés ou non, émanant des établissements d'enseignement et de recherche français ou étrangers, des laboratoires publics ou privés.

Massive formation of lawsonite in subducted sediments from the Schistes Lustrés (W. Alps): Implications for mass transfer and decarbonation in cold subduction zones

Benjamin Lefeuvre, Philippe Agard, Anne Verlaquet, Benoît Dubacq, Alexis Plunder



PII: S0024-4937(20)30266-8

DOI: <https://doi.org/10.1016/j.lithos.2020.105629>

Reference: LITHOS 105629

To appear in: *LITHOS*

Received date: 28 October 2019

Accepted date: 6 June 2020

Please cite this article as: B. Lefeuvre, P. Agard, A. Verlaquet, et al., Massive formation of lawsonite in subducted sediments from the Schistes Lustrés (W. Alps): Implications for mass transfer and decarbonation in cold subduction zones, *LITHOS* (2020), <https://doi.org/10.1016/j.lithos.2020.105629>

This is a PDF file of an article that has undergone enhancements after acceptance, such as the addition of a cover page and metadata, and formatting for readability, but it is not yet the definitive version of record. This version will undergo additional copyediting, typesetting and review before it is published in its final form, but we are providing this version to give early visibility of the article. Please note that, during the production process, errors may be discovered which could affect the content, and all legal disclaimers that apply to the journal pertain.



**Massive formation of lawsonite in subducted sediments from the Schistes Lustrés (W. Alps): implications for mass transfer and decarbonation in cold subduction zones**

Benjamin Lefeuvre<sup>1,\*</sup> benjamin.lefeuvre@sorbonne-universite.fr, Philippe Agard<sup>1</sup>, Anne Verlaquet<sup>1</sup>, Benoît Dubacq<sup>1</sup>, Alexis Plunder<sup>2</sup>

<sup>1</sup>Sorbonne Université, CNRS-INSU, Institut des Sciences de la Terre de Paris, ITeP UMR 7193, F 75005 Paris, France

<sup>2</sup>BRGM – Bureau des recherches géologiques et minières (BRGM). 3 avenue Claude Guillemin, 45000 Orléans, France

\*Corresponding author.

**ABSTRACT**

This study investigates the reactions allowing crystallization of large amounts of lawsonite ( $\text{CaAl}_2\text{Si}_2\text{O}_7(\text{OH})_2 \cdot [\text{H}_2\text{O}]$ ) found in calc-schists metamorphosed in a subduction zone setting. Previous studies of lawsonite-forming reactions in metasediments have highlighted its importance for the large-scale budget of  $\text{CO}_2$ , as the calcium required to form lawsonite is thought to originate from decarbonation reactions. Yet, thermodynamic modelling as well as isotopic measurements have indicated that 80 to 90% of the carbon is retained in sediments, and there is no evidence of major decarbonation in the field. As lawsonite contains abundant  $\text{H}_2\text{O}$  and has a large stability field, understanding its crystallization is also important to assess fluid migration and mass transfer in a critical part of the subduction system where slow earthquakes are nucleating (such as LFEs or ETS).

The upper units of the blueschist facies metasediments of the Schistes Lustrés complex (Western Alps), buried to depths of ~ 30-40 km, have been selected as an ideal case study as they host up to 40 vol.% of lawsonite. Lawsonite is found crystallized over several generations, in veins, in reaction fronts as well as in the rock matrix. Three types of lawsonite were identified. The most abundant type of lawsonite is associated with quartz and ankerite. This mineral assemblage formed from phyllosilicates and calcite in a continuous reaction: chlorite + calcite + kyanite = lawsonite + ankerite + quartz + H<sub>2</sub>O. According to thermodynamic modelling, this reaction is restricted to a narrow pressure-temperature domain and initiates around 180°C and 0.4 GPa. Lawsonite is also observed and predicted to grow from Fe-Mg-carpholite at higher metamorphic conditions. None of these reactions allow efficient net export of carbon, as one carbonate replaces another, and most observations are consistent with closed-system behaviour at outcrop-scale, in agreement with geochemical studies. At sample-scale and below, crystallization of lawsonite is linked to homogenization of carbonate and pelitic domains in geologically fast reactions. Dissolution of calcite produces reactive fluids prone to react with pelitic domains and crystallize lawsonite and another carbonate. Although metamorphic veins are ubiquitous to the upper units of the Schistes Lustrés Complex, most of them result from local reactions and do not indicate large-scale mass transfer.

Keywords: lawsonite, metasediments, fluid/mass transfer, decarbonation, Schistes Lustrés, seismogenic depths

## 1. INTRODUCTION

Sediments buried in subduction zones contain large amounts of volatiles (up to ~7 wt.% H<sub>2</sub>O and 30 vol.% carbonates according to Plank and Langmuir, 1998; Røa and Ruff, 1996; Clift, 2017). Understanding their behaviour is key to assess the fate of carbon and fluids in subduction settings (Gorman et al., 2006; Bebout, 2007; Cook-Collars et al., 2014; Kelemen and Manning, 2015; Dragovic et al., 2018; Plank and Manning, 2019). Metamorphosed sediments also play an important role along the subduction interface (Agard et al., 2018; Raimbourg et al., 2018): production and expulsion of metasediment-derived fluids is proposed to control the periodicity of slow earthquakes at the base of the seismogenic zone (and more specifically around depths of 35 km) through changes in permeability and dissolution-precipitation creep (Fig. 1a; Rogers and Dragert, 2003; Audet et al., 2009; Osei Tutu et al., 2018; Behr and Becker, 2018). The associated element mobility, metasomatism and changes in rheology must be extensive, for example Audet and Bürgmann (2014) suggest km-scale transfer of silica from metasediments to the overriding plate based on high compressional- to shear-wave velocity ratios ( $V_p/V_s$ ). The interplay between deformation, mineral reactions and

rheology along and above the plate interface, however, remains largely unknown (Breeding and Ague, 2002; Saffer and Tobin, 2011; Bebout and Penniston-Dorland, 2016).

One target outcropping unit to study this interplay is the Schistes Lustrés complex of the Western/Central Alps and Corsica (Figs. 1b-d), an accretionary prism including several units and subunits preserving seafloor material, i.e. calcschists, metapelites and remnants of crustal material (e.g., Tricart and Lemoine, 1986). Metamorphism of the Schistes Lustrés originates from subduction during closure of the Liguro-Piemontese ocean (see e.g., Lagabrielle and Lemoine, 1997). The selected area belongs to the uppermost units of the Schistes Lustrés complex, which experienced blueschist-facies metamorphism with peak conditions between 1.2 GPa – 300°C and 1.9 GPa – 450°C (yellow dots; Fig. 1d). Mass transfer via metamorphic fluids appears extensive, as shown by the presence of ubiquitous veins bearing high-pressure minerals (Goffé and Chopin, 1986; Agard et al., 2001b, 2009; Bousquet et al., 2002; Plunder et al., 2012; Vitale Brovarone et al., 2014).

A notable feature of the upper unit of the Schistes Lustrés complex is the high abundance of lawsonite ( $\text{CaAl}_2\text{Si}_2\text{O}_7(\text{OH})_2 \cdot [\text{H}_2\text{O}]$ ), commonly greater than 20 vol.% and frequently associated with quartz (Caron, 1974; Sicard-Lochon, 1987; Agard et al., 2000). With 12 wt.%  $\text{H}_2\text{O}$ , lawsonite is a major carrier of  $\text{H}_2\text{O}$ . Lawsonite is stable up to ultra-high pressures, implying it may release water at depths greater than 200 km in cold subduction zones (Schmidt and Poli, 1998, 1994; van Keken et al., 2011; Faccenda, 2014). Lawsonite allows for many cation exchanges, especially in its large Ca site prone to

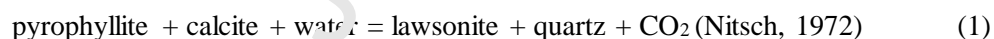
strain (Martin et al., 2011; Vitale Brovarone and Beyssac, 2014; Dubacq and Plunder, 2018). It is thought to play a key role in trace element cycling into the deep Earth (Schmidt and Poli, 1998, 1994; Zack and John, 2007; Tsujimori and Ernst, 2014; Fornash et al., 2019).

Yet the formation of lawsonite remains poorly understood and models are fraught with contradictions (see Clarke et al., 2006). Explaining large modal amounts of lawsonite in metasediments is problematic due to the low amounts of Ca initially present in pelitic rocks. Decarbonation and metasomatism are necessarily invoked processes, with a huge impact on modelling the mobility of carbon in its deep cycle (Kerrick and Connolly, 2001; Gorman et al., 2006; Kelemen and Manning, 2015; Stewart and Ague, 2018). Local accumulations of lawsonite in hybrid metasediments from Corsica ('lawsonitites'; >75 vol.%) have been interpreted as the result of large-scale metasomatism through serpentinite-derived metasomatic fluids, with and without decarbonation (Vitale-Brovarone et al., 2014; Piccoli et al., 2016; respectively).

In contrast to Corsican lawsonitites, the lack of significant isotopic shift in volatiles (C, O, H) from the Schistes Lustrés suggests limited external fluid infiltration, except possibly along tectonic contacts (Henry et al., 1996; Cook-Kollars et al., 2014; Collins et al., 2015; Jaeckel et al., 2018; Epstein et al., 2019). Fluid-mobile elements (e.g., H, N, B, Li, Ba, K, Rb, Cs) overall show little evolution along comparable rocks in the Cottian Alps (Busigny et al., 2003; Bebout et al., 2013; Barnes et al., 2019). Most fluids percolating through these rocks appear internally-derived and/or derived from similar

lithologies, in support of closed-system behaviour at the meter scale and possibly up to 100 meter-scale, at least for components other than H<sub>2</sub>O. This is in stark opposition to large-scale element mobility and extensive metasomatism.

Given the volumetric extent of the Schistes Lustrés metasediments, understanding the formation of lawsonite in terms of reactions, decarbonation, loss or gain of water and silica is crucial to quantifying the element budget along and across the plate interface. The lawsonite forming reaction is not readily accessible since lawsonite rarely hosts silicate mineral inclusions and is generally poorly preserved in exhumed rocks. Lawsonite is commonly pseudomorphed and replaced by a variety of minerals, including phyllosilicates (mostly chlorite and white mica) and epidote, during burial (as in Syros and Turkey: Hamelin et al., 2018; Fornash et al., 2019) and exhumation (e.g., in the Cottian Alps: Sicard-Lochon, 1987; Plunder et al., 2012). Reactions suggested so far for lawsonite crystallization in metasediments include:



Both reactions involve decarbonation and production of CO<sub>2</sub>, since Ca is mobilized from calcium carbonate. Lawsonite, however, was shown experimentally to be unstable in CO<sub>2</sub>-rich fluids (reaction 1 being valid for XCO<sub>2</sub><0.05; Nitsch, 1972). Based on thermodynamic modelling of reaction (2), Cook-Kollars et al. (2014) suggested that only moderate amounts (10-20 vol.%) of lawsonite could be produced given the bulk composition of the Schistes Lustrés and that the Schistes Lustrés retained 80 to 90% of their initial C content. Yet larger amounts of lawsonite pseudomorphs are found in most of these rocks (Caron, 1974; Sicard-Lochon, 1987), and whether lawsonite formation requires addition of H<sub>2</sub>O to the sediments or not is unknown. Based on field, mineralogical and micro-structural observations together with geochemical analysis, the present contribution documents lawsonite concentrations along a representative transect of the uppermost units of the Schistes Lustrés. This study aims at explaining how such concentrations have been reached. Mineral reactions forming lawsonite and the scales of associated fluid/mass transfer are critically discussed to shed light on the involvement of large-scale transfer, silica deposition, and decarbonation.

## 2. GEOLOGICAL SETTING

### 2.1 The Schistes Lustrés paleo-accretionary complex in the Alpine orogenic belt

The Schistes Lustrés complex belongs to the internal domain of the Alpine orogenic wedge (Figs. 1b,c, inset; for more details on the overall Alpine structure, see: Coward and Dietrich, 1989;

Lagabriele and Lemoine, 1997; Rosenbaum and Lister, 2005; Handy et al., 2010). The Western Alps formed as a result of east-dipping, slow and cold subduction ( $\sim 8^{\circ}\text{C}/\text{km}$  at a maximum 2 cm/year; Agard et al., 2001a; Le Pichon et al., 1988; Lapen et al., 2003) of the Valais and Liguro-Piemontese slow-spreading oceans (Lagabriele and Cannat, 1990). Oceanic subduction lasted from c. 100 to 40 Ma and was followed by continental subduction and collision of the European plate with Apulia.

The Schistes Lustrés complex is mostly made of metasediments of seafloor origin showing alternations of thinly bedded carbonate-rich and pelitic layers. It also contains slivers and blocks of various scales, more abundant in the lower units, of mafic and ultramafic bodies from the Liguro-Piemontese ocean (Fig. 1b; Lagabriele and Lemoine, 1985; Lagabriele et al., 2015). The Schistes Lustrés sediments were deposited from the Upper Jurassic ( $\sim 150$  Ma, De Wever and Caby, 1981) to the Late Cretaceous ( $\sim 70$ -65 Ma, Lemoine et al., 1986) and formed a 100-400 m thick sediment pile (De Wever and Caby, 1981). During subduction and exhumation, metasediments were intensely folded, leading to an important thickening of the initial sediment pile (Agard et al., 2002). Approximately 30 to 50% of the total sedimentary cover was eventually exhumed, much more than its oceanic basement ( $< 5\%$ ; Agard et al., 2009). Based on lithological differences in the Schistes Lustrés complex, three to four main units have been distinguished (Lagabriele, 1990; Deville et al., 1992; Fudral, 1996; Agard et al., 2001a; Tricart and Schwartz, 2006; Lagabriele et al., 2015). Plunder et al. (2012) showed that the upper, median and lower units experienced increasing metamorphic conditions.



Thermobarometric estimates show an eastward increase from the upper (1.2 GPa – 300°C west of Fraiteve) to the lower units (2.1 GPa – 500°C) as shown in figure 1d (Agard et al., 2001a; Beyssac et al., 2002; Plunder et al., 2012).

## 2.2 Tectono-metamorphic evolution along the Cottian Alps transect

The Schistes Lustrés complex recorded several deformation stages which are well constrained in terms of age and pressure-temperature (P-T) conditions (Agard et al., 2001a, 2002; Tricart and Schwartz, 2006). This study focusses on the upper unit of the Schistes Lustrés (LPU) along a ~15 km SW-NE traverse between Mt. Fraiteve and Colle delle Finestre, in the French-Italian Cottian Alps (Figs. 1b, c; Caron, 1974; Polino et al., 1984). Four deformation stages are recognized in the LPU (Agard et al., 2002). The first episode D1 is linked to peak or near-peak burial, as indicated by the crystallization of Fe-Mg-carpholite and lawsonite, and is thought to correspond to recumbent folding and thin-skinned stacking of several slices under blueschist facies conditions at ~60-50 Ma. Associated tectonic patterns are largely erased. A second fabric D2 is dated between 51 and 45 Ma and corresponds to early stages of exhumation under blueschist facies conditions (~1.2 GPa – 350°C in the area of Monte Triplex). It is marked by dominant top-to-the east shear senses. A third stage D3, characterized by top-to-the west ductile to brittle deformation in greenschist facies conditions (~0.7 GPa – 300°C), occurred between

38 and 35 Ma. The final stage D4 (and D5 identified in places) corresponds to brittle deformation marked by local extension, probably c. 28-20 Ma (Tricart and Schwartz, 2006).

### 3. FIELD CHARACTERIZATION AND SAMPLING

Lithologies and mineral abundances were investigated along the 15-km traverse through the LPU unit (Fig.1b). While detailed observations and sampling were carried out along the whole section, this study documents in greater details the ~200 m long Mt. Triple locality (Figs. 2, 3; metamorphic peak conditions of 1.6GPa – 350°C, Fig. 1d).

#### 3.1 Lithologies and distribution of hydrous metamorphic minerals

Figure 2 presents the five types of lithologies distinguished between carbonate-rich and pelite-rich layers in the LPU unit. Amounts of lawsonite and Fe-Mg carpholite vary systematically between rock types, although lithologies appear rather similar at first examination. The pelitic endmember (lithology 1) is composed of dark, organic-rich and phyllosilicate-rich material where carbonate layers are absent or not visible at the cm scale (Figs. 2a, b). By contrast, the carbonate endmember (lithology 5; Fig. 2a) consists of metric (1-5 m.) carbonate horizons, often with subordinate horizons containing phyllosilicates (<5 vol.%; Fig. 2b). Lithologies 2, 3 and 4 (hereafter referred to as calcschists) are composed of a mixture of pelitic layers and carbonate beds in various proportions (Figs. 2a, b). Lithology 2 contains thinly bedded, typically cm-scale carbonate layers in a shaly matrix (pelite to

carbonate volume ratio ~3:1). Lithology 3 shows regularly alternating pelitic and carbonate horizons with roughly equivalent thicknesses (commonly 5-10 cm, and up to ~20 cm). Lithology 4 is characterized by more compact calcschists in which phyllosilicate-rich layers do not exceed cm-scale (pelite to carbonate ratio ~1:3).

The metasediments contain significant amounts of hydrous minerals typical of blueschist facies metamorphism such as lawsonite and Fe-Mg-carpholite, or preserve evidence of their former presence. Fe-Mg-carpholite is much more sensitive to retrogression and alteration than lawsonite. Fe-Mg-carpholite is readily replaced by chlorite and white mica during exhumation and frequently only preserved as micrometric needles in quartz (Chopin and Goffé, 1986; Agard et al., 2001b). Lawsonite is commonly pseudomorphed, allowing for minimum estimates of its former abundance. Figure 2b displays modal amounts of lawsonite determined in the field. Lawsonite is present in all lithologies but mostly found in calcschists among which it is heterogeneously distributed: it makes up to 40 vol.% of rock type 3 (e.g., at Mt. Tripiex and Genevris). Fe-Mg-carpholite is mainly observed in lithology 1, although it may have occurred in other lithologies prior to retrogression. In general, these two minerals are not observed coexisting in hand specimen or thin-section. Along the transect between Mt. Fraiteve and the Assietta pass (Figs. 1b-c, 2c), most rock types correspond to lithologies 2, 3 and 4 (calcschists). Some locations present much more pelitic material classified as lithology 1 (Mt. Fraiteve and Assietta pass). The carbonate-rich endmember of our classification (lithology 5) is only sparsely

encountered; these rocks are found in greater proportions in (and are typical of) the median unit of the Schistes Lustrés further east.

### 3.2 Outcrop-scale observations in Triplex

Detailed petrological observations and sampling were performed along the 200 m long, relatively continuous and homogeneous exposures of Mt. Triplex (along the Port road and immediately to the west, Fig. 3). Sampling sites are shown on figure 3a. Observation and representative sampling were carried out with particular attention to ensure consistent scale transfer from the hm-scale (Figs. 3a, b) to the cm-scale (Figs. 3c-f, 4, 5, 6). Outcropping rocks are essentially made of lithology 2. They are pervasively deformed by hundred meter-long shear bands, with cm-scale penetrative shear structures (C/S or C' bands, vein rotations) consistent with top-to-the east deformation attributed to D2. These are interpreted as marking the onset of exhumation (Agard et al., 2001a). The main schistosity visible on figure 3 is a composite D1-D2 structural pattern. The D2 shear bands are cross-cut by later, ductile to brittle and mostly west-vergent planes, corresponding to the D3 deformation stage (Fig. 3d), which are locally east-vergent when reworking earlier D2 structures. Late, *en échelon* calcite  $\pm$  quartz  $\pm$  chlorite veins are associated with this D3 stage. Metasediments are highly deformed and show many m- to cm-scale folds of the schistose matrix, along with multiple vein generations. The carbonate layers (~30 vol.%) are heterogeneously distributed across the outcrop. Ankerite-rich reddish haloes are commonly observed between carbonate and pelitic horizons (Figs. 4a, b, d). Lawsonite is present in the schistose

host-rock (Figs. 3e, 4) and in quartz  $\pm$  ankerite veins (Fig. 3f). Lawsonite is by far the predominant metamorphic hydrous phase (rare Fe-Mg-carpholite pseudomorphs are found in some layers), locally up to 45 vol.% of the host rock.

#### 4. LAWSONITE TYPES

At macroscopic scale, three types of lawsonite have been characterized based on their texture, association with other minerals, and presence in the schistose matrix or high-pressure veins (Figs. 3e, f, 5). For simplicity, these different types are termed LwsA, LwsB and LwsC. The lettering does not imply cross-cutting relationship or relative chronology as these remain unclear, as detailed below.

##### 4.1 Calcschist lawsonite (LwsA in lithologies 2 and 3)

LwsA, by far the most common type of lawsonite in this area, is mostly found in pelitic calcschists interlayered with carbonate-rich horizons (Figs. 3e, 4a) and makes up to 30% of lithology 2 and 40% of lithology 3. In addition to lawsonite, the pelite-rich layers are commonly composed of quartz (20 to 30%), calcite (0 to 30%), ankerite (< 20%), phengite (< 20%), chlorite (< 10%) and organic matter found as inclusions (Figs. 4e, f, g). LwsA forms millimetric to centimetric black prisms (Figs. 4c-g), generally well-preserved, texturally associated with quartz and oxidized reddish ankerite (Fig. 4d). Ankerite is found in carbonate layers and all across the pelitic layers. Ankerite is particularly concentrated at the edge of folded carbonate-rich layers where it forms diffuse, centimetre-thick

domains along lithological contacts (Figs. 4a, b). Well-defined horizons of ankerite are less frequent (Fig. 4d). The association of LwsA and ankerite is maximum at the interface between carbonate and pelitic layers, and decreases towards pelitic domains and towards thick carbonate horizons. The textural relationships between LwsA and ankerite are best preserved in thin carbonate layers (Fig. 4d). Figures 4e-f-g show fractured, organic-matter-rich, dark lawsonite crystals overgrown with pale newly-formed lawsonite, indicating incremental growth. When pseudomorphed, LwsA is replaced by a mixture of chlorite, phengite and calcite, as described in previous studies (Sicard Lochon, 1987; Vitale-Brovarone et al., 2014).

#### **4.2 Lawsonite-bearing veins (LwsB and LwsC)**

The second type of lawsonite (LwsB) is observed in pluri-centimetric to metric quartz veins following the main schistosity (Fig. 5a). LwsB forms elongated, cream-coloured crystals with long axis parallel to vein selvages and aligned with quartz fibres (Figs. 5a-c). Crystal size reaches 20 cm long in places. LwsB shows incremental growth and also crystallized in pressure shadows around boudinaged quartz veins (Figs. 5c-e). Lawsonite and quartz often evidence ductile deformation in LwsB-bearing veins (Fig. 5d), advocating for syn-deformation incremental growth and mode II vein opening. LwsB is generally only associated with quartz, but ankerite crystals have been observed in places, in particular in the vicinity of pelitic horizons (Fig. 5e). The third type of lawsonite (LwsC) is observed in millimetric to centimetric tensile veins (Fig. 5f, g) cutting across the host rock. They show the same

cream-coloured, elongated fibres as LwsB-bearing veins but are systematically associated with ankerite and quartz. The LwsC-bearing veins are particularly abundant in calcschists hosting LwsA and mostly located around fold hinges (in extrado domains) and near larger LwsB-bearing quartz veins. LwsC-ankerite-quartz fibres are perpendicular to the vein walls and these veins are dominated by mode I opening (Figs. 5f, g). Sometimes, these veins cross-cut LwsB-bearing veins and apparently opened in a single stage, possibly indicating shorter-lived tensile events than for LwsB formation. Early veins transposed along the schistosity have been identified in places as former, strongly deformed LwsC-bearing veins, suggesting that only the latest generation of LwsC-bearing veins is observed. Local accumulations of LwsB- and LwsC-bearing veins are found in m-scale domains scattered around Mt. Triplex, in lithologies where LwsA is also abundant (Figs. 3d, f).

## 5. PETROGRAPHY AND MINERALOGY

### 5.1 Textural relationships

In the calcschists, LwsA forms euhedral rhombi to oval crystals (Figs. 6a, d, e). Inclusions of organic matter, responsible for the black colour of hand specimens, are concentrated in LwsA cores (Figs. 4e-g, 6d). These inclusions form trails related to deformation accompanying burial and may record early episodes like D1 (Caron, 1974). Inclusion trails are found in adjacent crystals of lawsonite and ankerite (Fig. 6a). As for outcrop-scale observations, systematic relationships are found between

lawsonite, ankerite and quartz. These three minerals are commonly found in apparent textural equilibrium (Fig. 6) and included in one another: figure 6f shows LwsA and quartz included in rhombic ankerite crystals, and figure 6c shows ankerite and quartz included in lawsonite (see also Sup. mat.1, 3). The calcite - chlorite assemblage cross-cuts domains with lawsonite, ankerite and quartz. In carbonate-rich layers, the habitus of LwsA is different from that in the adjacent pelite-rich schist (Figs. 6b, c). Crystals are much smaller, better preserved and do not contain organic matter inclusions. Lawsonite crystals in veins never contain organic matter inclusions. Fine-scale alternations of LwsC, quartz and ankerite are observed along small veins, highlighting their close association and co-crystallization. Lawsonite is only partially preserved in LwsC veins (LwsB is better preserved in veins). Crystals of LwsC are fractured, replaced and pseudomorphed by a fine mixture of chlorite, phengite and calcite along cracks.

The amounts of ankerite and lawsonite were estimated for LwsA, LwsB and LwsC-bearing thin sections from optical microscopy images (Fig. 7). LwsA-bearing rocks show Lws/Ank ratios varying around 1.5. Vein samples with LwsB and LwsC show more scattered ratios, between 1 and 3 for LwsB and 0 and 1 for LwsC. Since LwsC are much more overprinted by phengite and chlorite than LwsA, the LwsC/Ank ratios were corrected using pseudomorphs (see Sup. mat. 2). The corrected LwsC/Ank estimates plot around 1.5, as for LwsA/Ank. Large variations in LwsB/Ank ratios reflect the largely varying amounts of ankerite (Figs. 7, 5a, e). Most phyllosilicates appear linked to peak or retrograde



metamorphism. Phengite appears in the main foliation as well as cross-cutting it. Chlorite is found in lawsonite pseudomorphs together with phengite and calcite, a typical lawsonite retrogression reaction in the SL (Sicard-Lochon, 1987). Chlorite is also found as retrogression product between lawsonite and ankerite.

## 5.2 Rock and mineral composition

Whole-rock major element chemistry was performed with an Agilent 5100 ICP-OES at the ALIPP6 analytical facility (Sorbonne Université, Paris) after acid attack of finely-ground samples. A HF-HNO<sub>3</sub> mixture was used for dissolution of samples in closed tubes over 24 hours, and boric acid added immediately after opening to prevent loss of silicon. Dilution and measurement followed shortly (within 24 hours). Analytical uncertainties are estimated to be better than 5% of the measured value. Loss on ignition was obtained by mass loss after heating approximately 4 grams of samples at 110°C for one night for adsorbed water and at 1000°C for three hours for remaining volatiles. Mineral analysis was carried out at the CAMPARIS facility (Sorbonne Université, Paris) with a CAMECA SX-FIVE electron microprobe and the data reducing method of Pouchou and Pichoir (1991). Analytical conditions were 15 kV-10 nA in WDS mode, for analysis of major elements. Conditions were changed to 25 kV and 100 nA when measuring Sr and Ti, which are in low concentrations. Fe<sub>2</sub>O<sub>3</sub> (Fe), MnTiO<sub>3</sub> (Mn, Ti), diopside (Mg, Si), Cr<sub>2</sub>O<sub>3</sub> (Cr), orthoclase (Al, K), anorthite (Ca) and albite

(Na) were used as standards for elements in parentheses. Representative analyses are provided in Table 1 for lawsonite. All Fe is assumed to be in divalent state and is expressed as FeO.

Figure 8a shows the composition of ankerite, chlorite and white mica. Variations in minor to trace element concentrations of lawsonite are shown in figures 8b, c, d. Figure 9 shows selected chemical maps for major and minor to trace elements. Ankerite shows a composition close to the ideal  $\text{Ca}_1\text{Fe}_{0.5}\text{Mg}_{0.5}(\text{CO}_3)_2$  with very constant Fe/Mg ratio around 1 (Fig. 8a; Table 1). In places, Mn zoning is observed (Fig. 9d), with rims enriched in Mn. White micas are of muscovite and phengite type (Fig. 8a), a solid solution between muscovite and celadonite with minor (~10%) pyrophyllite content. Crystals with the highest celadonite content probably preserve the high pressure equilibrium stage (Agard et al., 2001b). Chlorite is fairly homogeneous and compares well with previous data, plotting in a restricted composition interval of Figure 8a at low sudoite content. The Mg/Fe ratio of chlorite is similarly homogeneous. Together with textural evidence, this points to chlorite being mostly retrograde (Fig. 9a). Lawsonite is close to its ideal composition, and no difference in major elements was found between the various lawsonite types and samples. Variations in trace amounts of Ti and Sr were detected (Figs. 8b, c, d, 9b, c; Table 1). Optically-zoned LwsA appears also zoned in Ti and shows higher Ti content in the core, linked to hour-glass zoning (Figs. 8b, 9b; see Sup. mat. 3). Crystals of LwsA also show enrichment in Sr at their rims, while LwsA cores are Sr-poor (Figs. 8b, 9b, c). Similarly, LwsC crystals are either slightly enriched in Ti or in Sr (Fig. 8d). Only LwsB can

reach higher Sr contents and contain both Sr and Ti (Fig. 8c). The close association of lawsonite, ankerite and quartz is readily apparent from chemical mapping (Fig. 9a).

## 6. DISCUSSION

### 6.1 Co-crystallization of lawsonite and ankerite

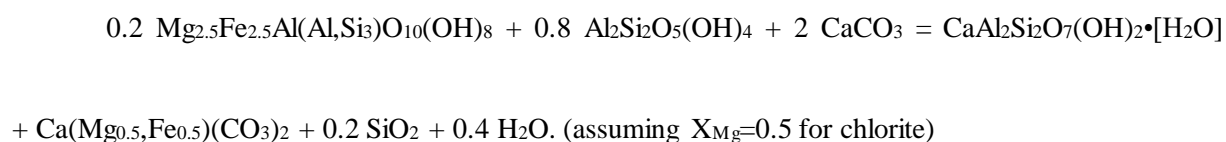
Co-crystallization of lawsonite, quartz and ankerite is supported by their close association, both as intricate, parallel fibres seeded in vein walls (LwsC; Figs. 5f, g) and in the host-rock (LwsA-rich domains, Figs. 4, 6). The abundance of lawsonite in pelitichists (lithologies 2 and 3) with mixed carbonate-rich and pelite-rich layers is consistent with the fact that the latter contain most of the cations needed for lawsonite crystallization, i.e. Al, Si, H. Calcium, however, is not present in sufficient amounts in pelite-rich layers to explain the formation of up to 30-40 vol% of lawsonite. This requires adding massive amounts of Ca to pelitic domains via either (i) infiltration of external Ca-rich fluids, (ii) local decarbonation and/or (iii) reaction between carbonate and pelitic layers.

The first hypothesis is not supported by isotope data on C-O-H which should be concomitantly altered (Henry et al., 1996; Cook-Kollars et al., 2014). Field and petrographic evidences do not support significant decarbonation: there is crystallization of ankerite and overall no major dissolution of carbonate. The third hypothesis is favoured: replacement of primary calcite from the carbonate-rich lithologies by ankerite allows substituting half of the initial Ca amount with Fe and Mg, with zero net

export of carbon. The net reaction releases sufficient Ca to form lawsonite in the more pelitic layers from mixed lithologies. An indication on the spatial range of element transfer is provided by the very low content of lawsonite in pelitic lithologies with no carbonate horizon within a few meters (almost zero in lithology 1).

Element transfer through dissolution-precipitation reactions explains the systematic association of lawsonite with ankerite at all scales (e.g., Figs. 4a-d, 5f, g, 6b-f) and the presence of ankerite haloes between pelitic and carbonate horizons (Figs. 4a, b). Based on (i) observations from this study and former descriptions (Caron, 1974; Sicard-Lochon, 1986; Caron et al., 1987), in particular that reactants may have been somewhat similar to minerals overgrowing lawsonite and ankerite on exhumation (i.e., chlorite, calcite Fig. 9a), and (ii) the large amounts of hydrous aluminosilicates present in common sediments (Planck and Langmuir, 1998), lawsonite and ankerite are expected to form at the expense of chlorite, calcite and kaolinite, themselves formed at the expense of former detrital and early diagenetic phases. The observed overall 1.5 volume ratio of lawsonite to ankerite (controlled by LwsA-bearing rocks) corresponds to a 1:1 Lws/Ank molar ratio. This points to a reaction such as:

chlorite + kaolinite + aragonite = lawsonite + ankerite + quartz + water (3)



## 6.2 Thermodynamic modelling of formation of the lawsonite-ankerite assemblage

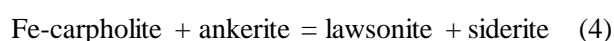
In order to locate reaction (3) in P-T space, a first pseudosection was computed using a bulk composition corresponding to the stoichiometry of reaction (3) assuming excess water in the CaFMASHC system (Fig. 10a). Computations were made using Perple\_X version 6.8.4 with the updated database of Holland and Powell (1998) and corresponding solution models (for chloritoid, dolomite, Fe-Mg-carpholite, phengite) except for chlorite (after Holland et al., 1998). As shown on figure 10a, during burial along a 8°C/km metamorphic gradient, the lawsonite-forming reaction starts at 170°C and 0.44 GPa (i.e., ~15 km depth) and is completed across a restricted P-T range ending at 190°C (Fig. 10b). This reaction forms ~60 vol.% of lawsonite. In this case all lawsonite crystals would be formed during a continuous reaction occurring over a short period of time (a minimum of ~250 000 years at a convergence rate of 2 cm yr<sup>-1</sup>).

In order to quantify the extent to which lawsonite and ankerite may co-crystallize from the interaction between carbonate and pelitic-rich layers, the mineralogical evolution of the calcschists has been modelled in the KCaFMASHC system using the same thermodynamic set up and water saturated conditions. Two pseudosections were built using compositions representative of typical pelitic and carbonate-rich domains (i.e., on either side of the lithological boundary shown in figure 4a). Sample SL16-11c, a type 3 calcschist from Mt. Triplex, was separated in pelitic (R11SCH) and carbonate-rich (R11CARB) domains. For these two bulk rock compositions, CO<sub>2</sub> and H<sub>2</sub>O are declared as

components. CO<sub>2</sub> content is inferred from the CaO content, assuming that carbonates host all the CO<sub>2</sub> of the rock. H<sub>2</sub>O content is fixed at 8 wt.% in R11SCH and 5.2 wt.% for R11CARB. These values ensure water saturation across the whole P-T domain, yet represent the minimum H<sub>2</sub>O content to reach water saturation at low P and T conditions. They are fixed to allow chlorite and kaolinite to form at  $P-T \leq 0.2 \text{ GPa} - 150^\circ\text{C}$  while minimizing the amount of stilbite which take over for greater H<sub>2</sub>O contents (see Sup. mat. 4). The amount of stilbite in itself does not affect the stability field of lawsonite but the presence of excessive stilbite (hosting Ca instead of calcite) would imply an additional lawsonite-forming reaction with addition of CO<sub>2</sub>, which was deemed unlikely. It is also noted that H<sub>2</sub>O and CO<sub>2</sub> are immiscible at these conditions (so that presence of CO<sub>2</sub> will not modify water activity, equal to 1 here) and that the mixing model of Holland and Powell (2003) does not reproduce this accurately (see Dubacq et al., 2013). The water content does not affect significantly phase relations at higher grade. It is stressed that the lingering presence of detrital minerals, unobserved in the present rocks but likely dominant in the lowest-grade parts of the pseudosections, will have a greater impact on the reactions experienced by the rocks than details of the modelling before appearance of lawsonite.

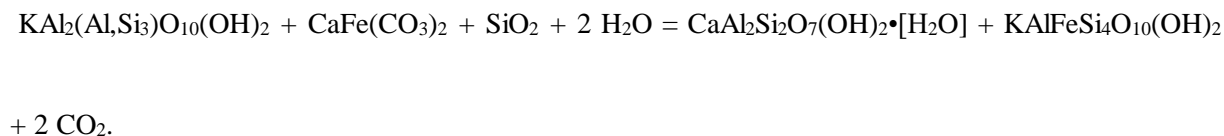
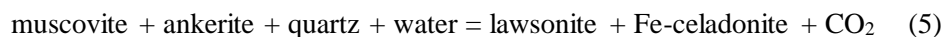
Pseudosections predict up to 34 vol.% of lawsonite for the pelitic domains and 23 vol.% for carbonate-rich domains at peak burial conditions (1.6 GPa and 350°C; Figs. 10c, d). Calculated Lws/Ank volume ratios are close to 1.5 in both cases but this ratio increases slightly close to peak conditions for the pelitic domain. Most of the lawsonite forms through reaction (3) with ankerite and quartz at the

expense of chlorite, kaolinite and calcite, which releases water. This mechanism predominates in carbonate-rich domains. In pelitic domains, lawsonite formation continues during breakdown of kaolinite and chlorite, which is expected to form Fe-Mg-carpholite above 210°C. Above 330°C, a continuous reaction forms lawsonite and siderite from Fe-Mg-carpholite (which provides Al and Si) and ankerite (which becomes the source of Ca after exhaustion of calcite, Figs. 10c, e). The corresponding reaction, written for end-members in the CaFASHC system for simplification, is:

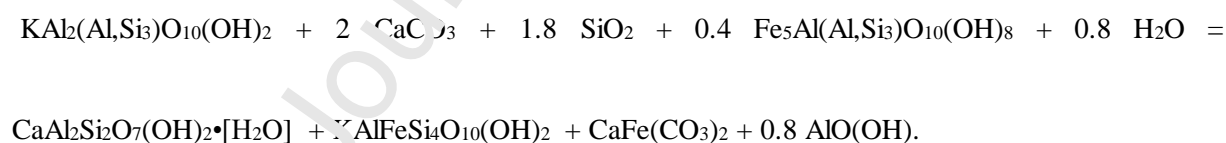
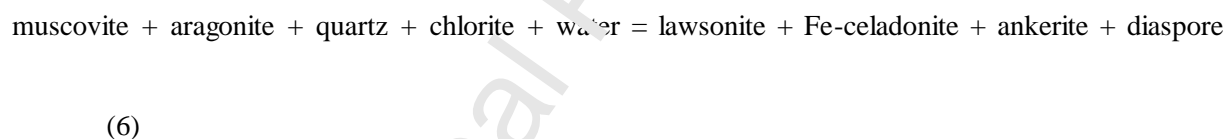


Note that in reaction (4), Fe-Mg-carpholite is the mineral consumed: in addition to being much more sensitive to retrogression and alteration than lawsonite, this may explain why both minerals are very rarely found in equilibrium (Plunder et al., 2013). Further quartz production accompanies to the disappearance of kaolinite above 310 °C (Fig. 10e).

The Tschermak exchange in micas ( $2 \text{Al}^{3+} = (\text{Mg}^{2+}, \text{Fe}^{2+}) + \text{Si}^{4+}$ ), which releases Al and consumes Mg, Fe and Si at constant amount of mica, could also contribute to lawsonite formation, as proposed by Cook-Kollars et al. (2014). In pelite-rich domains, the reaction, balanced here for phengite end-members in the KCaFASHC system, would produce  $\text{CO}_2$  and consume  $\text{H}_2\text{O}$ , as suggested by Cook-Kollars et al. (2014):



However, such reaction is not supported in our modelling, as shown by the parallel modal evolution of lawsonite, ankerite and quartz until 330°C (Fig. 10e). In carbonate domains, the continuous reaction producing small amount of lawsonite and ankerite above 180°C consumes quartz as well as chlorite and aragonite (as in reaction (3)). Considering that Al is provided by the Tschermak exchange in micas, the reaction would consume H<sub>2</sub>O but not release CO<sub>2</sub>:



Presence of white mica is common in lawsonite-bearing rocks, both as high-pressure phengitic mica and as retrogression products (see Sicard-Lochon, 1986; Agard et al., 2002; Hamelin et al., 2018 among others). However it is noteworthy that the Tschermak exchange is limited here, even in the high-pressure phengites (Fig. 8a), showing that reactions (5) and (6) are subordinate to reactions (3) and (4).



### 6.3. How progressive is lawsonite crystallization?

The large amounts of lawsonite observed in the Triplex area and lawsonite-ankerite relative proportions point to reaction (3) being prominent. Reaction (3) would account for the formation of most of the massive amounts of lawsonite in the Schistes Lustrés, especially LwsA. The relatively small P-T domain over which reaction (3) takes place suggests one large pulse of crystallization. Overstepping may increase this character by delaying nucleation of lawsonite and favouring faster growth due to a large distance to equilibrium. However this reaction is a medium to high-entropy reaction producing free fluid:  $\Delta S^0_r \approx -2.3$  J/K or  $-2.5$  J/L per mole of oxygen for Mg and for Fe end-members, respectively. This entropy production is  $\sim 5$  times larger than the andalusite-sillimanite reaction (using the database of Holland and Powell, 2011). Reaction (3) is therefore unlikely to be largely overstepped (see Pattison et al., 2011). The carpholite-consuming reaction (4) appears more sensitive to overstepping ( $\Delta S^0_r \approx 1.5$  J/K per mole of oxygen; no fluid production) but continuous lawsonite growth may have benefited from the presence of lawsonite crystals nucleated during reaction (3). In addition, deformation during early stages of burial will increase chances of lawsonite crystallization.

Rapid growth of lawsonite is supported by hourglass Ti zoning in LwsA cores (Figs. 4e-g, Sup. mat.

3). Preferential incorporation of Ti on some crystal faces has been related to out-of-equilibrium Ti incorporation (Dowty, 1976) and compares to sector zoning implying fast growth for lawsonite (Ueno,

1999; Vitale-Brovarone et al., 2014). Rapid growth is also supported by the thin, cm-scale reaction fronts (Fig. 4d) showing high reactivity of the fluid (large Damköhler number, the ratio of reaction rate to element advection rate in fluids; see Skelton et al., 1997; Wigley et al., 2013). In this view the production of lawsonite appears transport-limited.

Therefore the restricted P-T window (hence time) over which lawsonite crystallized is likely underestimated by equilibrium modelling and reaction (3) may be more progressive. First, rock compositions considered in the modelling may represent already evolved or mixed lithologies rather than the exact initial protoliths. Instead, calcium may not be readily available in pelite-rich domains, depending on the distance to carbonate layers (i.e., carbonate/pelitic layers alternation), thus transport mechanisms may significantly delay lawsonite crystallization. Around 200°C, cation diffusivity is sluggish yet at least five orders of magnitude faster in free fluid than grain boundary diffusion (e.g., Carlson, 2010; Verlaque et al., 2016). Therefore the presence of free fluids in otherwise isolated carbonate domains will be key to initiating reactions. Lawsonite-bearing veins also attest the presence of a free fluid phase. It is noteworthy that dehydration of smectite and replacement by illite, precursor to phengitic mica, provides water in pelitic domains over this temperature range (Vidal and Dubacq, 2009).

This points in turn to additional lawsonite-forming reactions not considered in the modelling. Detrital phases such as feldspar and clay minerals are expected at conditions below appearance of lawsonite.

Their breakdown to mineral assemblages including lawsonite will be progressive. In particular in pelitic domains, the smectite - illite - phengitic mica transition may contribute as a source of Fe and Mg to form ankerite and lawsonite from calcite, as in reaction (3), enlarging the P-T field of lawsonite crystallization. This is estimated as subordinate to reaction (3) because chlorite typically contains 10 to 25 times more Fe and Mg than illitic clays equilibrated around 200°C (Dubacq et al., 2010, their figure 2).

In summary, an array of evidence points to fast initial growth of lawsonite at moderate pressure, at least for most of LwsA (cores), which makes up a large volumetric proportion of lawsonite. More progressive events of crystallization and growth of lawsonite along the prograde path are attested and tentatively set in the frame of deformation events below.

#### **6.4 Different lawsonite types and veins: nature and timing of crystallization**

- LwsA: The large amounts of LwsA in pelitic layers (Fig. 3) are consistent with relatively rapid lawsonite growth, possibly as early in the burial history as around 0.4 GPa (Fig. 10). LwsA crystals also evidence incremental growth during deformation as shown by the trails of organic matter preserved in their cores and rotation of the cores with respect to the inclusion-free crystals (Figs. 4e-g, 6d; see also Caron, 1974). This event is possibly associated with D1 deformation phase (Agard et al., 2002). Deformation analysis is unfortunately complicated by the succession of deformation stages and

strain localization in the rheologically weak pelitic layers (Agard et al., 2002). Rapid and incremental growth could result from response to rearrangement of porosity, fluid pressure fluctuations and/or seismic cycles (Fagereng et al., 2011; Viete et al., 2018; Ganzhorn et al., 2019).

- LwsC: Small (<5 cm) tensile veins hosting LwsC are best preserved around D2 folds (Figs. 11a, 3d, 5f-g). These veins contain all products of reaction (3), i.e. lawsonite-ankerite-quartz, in proportions similar to those modelled in pseudosections and with textures evidencing co-crystallization before transposition into the S2 schistosity (Figs. 5, 11c, d). The mineralogical homogeneity of LwsC veins is interpreted as reflecting growth during progressive deformation, along the prograde path and from reaction (3), in deformation-controlled sites. These tensile veins evidence mode I opening and point to short-lived events, possibly repeated over time (through a delayed reaction (3)? Figs. 11d, 12a). Such fibrous veins are commonly interpreted as the result of mineral growth in volumetrically limited fluid-filled dilating space (Bons, 2000; Oliver and Bons, 2001; Verlaquet et al., 2011; Fisher and Brantley, 2014). The constant width of fibres across the vein indicates that crystals grew at the same rate, independent on the mineral or nuclei orientation, suggesting that their growth was limited by the vein opening rate. The earliest LwsC veins have probably been largely transposed into the schistosity.

- LwsB: Veins hosting LwsB generally lack ankerite or only in subordinate and variable amounts. The fact that LwsB veins do not show products of reaction (3) (unlike LwsC veins), suggests that LwsB-bearing veins formed either during replacement of ankerite and carpholite (e.g., through reaction (4),

>330°C on figures 10c, 12a) and/or by pressure solution of lawsonite, in the presence of either local or external fluids. The latter is supported by the growth of some LwsB in pressure shadows around former quartz vein boudins. These veins are by far larger and longer (>5-10 cm) than LwsC veins. They evidence boudinage stretching and internal rotation (Fig. 5a) indicative of formation throughout progressive deformation.

As a final note, the initial boundaries between the carbonate and pelitic layers are attenuated through deformation and migration of reaction fronts (Fig. 11b). This contributes to the progressive chemical mixing of the subducted sediment at the local scale, enhancing the stability of carbonates.

## 6.5. Implications for mass transfer and the carbon budget in subduction zone

The major lawsonite-in reaction reported here (reaction (3)) for the first time allows explaining the high lawsonite content observed in the calcschists. Importantly, the mineralogical and petrological evolution indicates that no significant decarbonation took place during lawsonite formation in the Schistes Lustrés calcschists up to 1.6 GPa (maximum pressure in Triplex area). Calcite dissolution led instead to local co-crystallization of lawsonite and ankerite during relatively fast reactions. In the debate on how much carbon is recycled to subarc depths or even beyond into the deep mantle (i.e., significant: Gorman et al., 2008; Cook-Kollars et al., 2014; Epstein et al., 2019; minor: Kelemen and

Manning, 2015), the results of this study show that there is no major decarbonation of slab sediments at least to depths of ~40km.

Further, in our samples, early-crystallized lawsonite stored much organic matter as inclusions, leading to minimum C export from the rock, at least until 35-40 km depth (Fig. 12). Assemblages bearing LwsA and LwsC imply that C remained within centimetres of its dissolution site, consistent with the isotopic signatures of C, O and H (Henry et al., 1996; Cook-Kollars et al., 2014; Collins et al., 2015; Jaeckel et al., 2018). There is also no evidence of carbonation by external C-enriched fluid as reported in ultramafic horizons in Alpine Corsica (Piccoli et al., 2016).

Intense veining together with the high abundance of water-rich minerals are direct witnesses of high fluid activity in the Schistes Lustrés. Externally-derived fluids contribute to pervasive, cm-scale element transfer between pelite and carbonate-rich domains (Figs. 4a,b), attenuating lithological contrasts (Figs. 11b, c) and restricting the scale of carbon mobility (black and blue boxes on figure 12b). Excess fluids may nevertheless be expelled into larger-scale vein networks (i.e., LwsB-bearing veins; blue arrows on figure 12b), possibly contributing to migration of fluids, silica and volatiles beyond the cm-m-scale.

Large-scale silica production at seismogenic depths was hypothesized to account for high Vp/Vs ratios (Figs. 11d, 12; Audet and Bürgmann, 2014). Lawsonite-quartz-bearing veins and reaction (3) do show mobilization and production of quartz. However, observations of the bulk mineralogy and

thermodynamic modelling imply small amounts of quartz produced, as silica is consumed in other reactions such as the Tschermak exchange of phengitic micas. There is also no field evidence for massive addition of silica via quartz veins, and none was detected by whole-rock chemistry (Henry et al., 1996). We conclude that large-scale silica migration is not likely in paleo-subduction complexes hosting Tethyan-type metasediments such as the Schistes Lustrés.

## 7. CONCLUSIONS

This study shows that the mineralogical evolution and voluminous formation of lawsonite during prograde metamorphism of the Schistes Lustrés complex indicate element redistribution mediated by fluids from low-grade metamorphic conditions (180°C, 0.4 GPa) to seismogenic depths (Fig. 12b). Lawsonite mostly grows in stoichiometric proportions with ankerite and quartz from calcite and phyllosilicates. Stabilization of a carbonate phase during lawsonite formation precludes any significant decarbonation of the calc-schists. While large amounts of fluids are involved, these results are consistent with the Schistes Lustrés complex behaving mostly as a closed system at the m-scale, in agreement with previous studies. Generalized mobilization of elements and dissolution/crystallization of water-rich phases set up rapid reactions leaving a wealth of small reaction fronts and veins consistent with local redistribution. In this view most of the lawsonite crystallized in a relatively short period of time from a continuous reaction in a narrow P-T field. One type of lawsonite-bearing vein

(LwsB) is consistent with progressive and incremental crystallization, and potentially larger transport distances, but is found in lesser amounts.

## Acknowledgements

This work was financially supported by the CNRS-INSU SYSTER programs, by ISTeP and by the ZIP project (REA grant agreement no. 604713 (ZIP “Zooming In between Plates”) from the People Programme (Marie Curie Actions) of the European Union’s Seventh Framework Programme FP7/2007-2013). We thank C. Loudouma and D. Deldique for their expertise with SEM characterisation; M. Fialin and N. Rividi for help with EPMA; B. Caron and B. Villemant for ICP-OES measurements; E. Delairis for making the thin sections and H. Raimbourg and L. Jolivet for discussions. We also thank P. Goncalves and B. Dragovic for their constructive reviews, which helped clarify the manuscript.



## Declaration of interests

The authors declare that they have no known competing financial interests or personal relationships that could have appeared to influence the work reported in this paper.

## REFERENCES

- Agard, P., Goffé, B., Touret, J.L.R., Vidal, O., 2000. Retrograde mineral and fluid evolution in high-pressure metapelites (Schistes lustrés unit, Western Alps). *Contributions to Mineralogy and Petrology* 140, 296–315.
- Agard, P., Jolivet, L., Goffé, B., 2001a. Tectonometamorphic evolution of the Schistes Lustrés complex: implications for the exhumation of HP and UHP rocks in the western Alps. *Bulletin de la Société Géologique de France* 172, 617–636.
- Agard, P., Vidal, O., & Coffin, B., 2001b. Interlayer and Si content of phengite in HP–LT carpholite-bearing metapelites. *Journal of Metamorphic Geology*, 19(5), 479–495.
- Agard, P., Monié, P., Jolivet, L., Goffé, B., 2002. Exhumation of the Schistes Lustrés complex: in situ laser probe  $^{40}\text{Ar}/^{39}\text{Ar}$  constraints and implications for the Western Alps. *Journal of metamorphic Geology* 20, 599–618.
- Agard, P., Plunder, A., Angiboust, S., Bonnet, G., Ruh, J., 2018. The subduction plate interface: rock record and mechanical coupling (from long to short timescales). *Lithos* 320, 537–566.
- Agard, P., Yamato, P., Jolivet, L., Burov, E., 2009. Exhumation of oceanic blueschists and eclogites in subduction zones: Timing and mechanisms. *Earth-Science Reviews* 92, 53–79. doi:10.1016/j.earscirev.2008.11.002
- Audet, P., Bostock, M.G., Christensen, N.I., Peacock, S.M., 2009. Seismic evidence for overpressured subducted oceanic crust and megathrust fault sealing. *Nature* 457, 76–78. doi:10.1038/nature07650
- Audet, P., Bürgmann, R., 2014. Possible control of subduction zone slow-earthquake periodicity by silica enrichment. *Nature* 510, 389–392. doi:10.1038/nature13391

- Barnes, J.D., Penniston-Dorland, S.C., Bebout, G.E., Hoover, W., Beaudoin, G.M., Agard, P., 2019. Chlorine and lithium behavior in metasedimentary rocks during prograde metamorphism: A comparative study of exhumed subduction complexes (Catalina Schist and Schistes Lustrés). *Lithos* 336, 40–53.
- Bebout, G.E., 2007. Metamorphic chemical geodynamics of subduction zones. *Earth and Planetary Science Letters* 260, 373–393.
- Bebout, G.E., Agard, P., Kobayashi, K., Moriguti, T., Nakamura, E., 2013. Devolatilization history and trace element mobility in deeply subducted sedimentary rocks: Evidence from Western Alps HP/UHP suites. *Chemical Geology* 342, 1–20. doi:10.1016/j.chemgeo.2013.01.009
- Bebout, G.E., Penniston-Dorland, S.C., 2016. Fluid and mass transfer at subduction interfaces - the field metamorphic record. *Lithos* 240–243, 228–258. doi:10.1016/j.lithos.2015.10.007
- Behr, W.M., Becker, T.W., 2018. Sediment control on subduction plate speeds. *Earth and Planetary Science Letters* 502, 166–173. doi:10.1016/j.epsl.2018.08.057
- Beyssac, O., Goffé, B., Chopin, C., Rouzaud, J.N., 2002. Raman spectra of carbonaceous material in metasediments: a new geothermometer. *Journal of metamorphic Geology* 20, 859–871.
- Bons, P.D., 2000. The formation of veins and their microstructures. *Journal of the Virtual Explorer* 2, 12.
- Bousquet, R., Goffé, B., Vidal, O., Oberhänsli, R., Patriat, M., 2002. The tectono-metamorphic history of the Valaisan domain from the Western to the Central Alps: New constraints on the evolution of the Alps. *Geological Society of America Bulletin* 114, 207–225.
- Breeding, C.M., Ague, J.J., 2002. Slab-derived fluids and quartz-vein formation in an accretionary prism, Otago Schist, New Zealand. *Geology* 30, 499–503.
- Busigny, V., Cartigny, P., Philippot, P., Ader, M., Javoy, M., 2003. Massive recycling of nitrogen and other fluid-mobile elements (K, Rb, Cs, F) in a cold slab environment: evidence from HP to UHP oceanic metasediments of the Schistes Lustrés nappe (western Alps, Europe). *Earth and Planetary Science Letters* 215, 27–42. doi:10.1016/S0012-821X(03)00453-9
- Carlson, W.D., 2010. Dependence of reaction kinetics on H<sub>2</sub>O activity as inferred from rates of intergranular diffusion of aluminium: Reaction kinetics and aluminium diffusion. *Journal of Metamorphic Geology* no-no. doi:10.1111/j.1525-1314.2010.00886.x
- Caron, J.M., 1974. Rapports entre diverses “générations” de lawsonite et les déformations dans les Schistes lustrés des Alpes cottiennes septentrionales (France et Italie). *Bulletin de la Société Géologique de France* 255–263.
- Caron, J.M., Potdevin, J.L., Sicard, E., 1987. Solution-deposition processes and mass transfer in the deformation of a minor fold. *Tectonophysics* 135, 77–86.
- Chopin, C., Henry, C., Michard, A., 1991. Geology and petrology of the coesite-bearing terrain, Dora Maira massif, Western Alps. *ejm* 3, 263–292. doi:10.1127/ejm/3/2/0263
- Chopin, C., Goffé, B., 1986. High-pressure metamorphism in the Western Alps : zoneography of metapelites, chronology and consequences. doi:10.5169/SEALS-50880
- Clarke, G.L., Powell, R., Fitzherbert, J.A., 2006. The lawsonite paradox: a comparison of field evidence and mineral equilibria modelling. *Journal of Metamorphic Geology* 24, 715–725. doi:10.1111/j.1525-1314.2006.00664.x

- Clift, P.D., 2017. A revised budget for Cenozoic sedimentary carbon subduction: Cenozoic Carbon Subduction. *Reviews of Geophysics* 55, 97–125. doi:10.1002/2016RG000531
- Collins, N.C., Bebout, G.E., Angiboust, S., Agard, P., Scambelluri, M., Crispini, L., John, T., 2015. Subduction zone metamorphic pathway for deep carbon cycling: II. Evidence from HP/UHP metabasaltic rocks and ophiicarbonates. *Chemical Geology* 412, 132–150. doi:10.1016/j.chemgeo.2015.06.012
- Cook-Kollars, J., Bebout, G.E., Collins, N.C., Angiboust, S., Agard, P., 2014. Subduction zone metamorphic pathway for deep carbon cycling: I. Evidence from HP/UHP metasedimentary rocks, Italian Alps. *Chemical Geology* 386, 31–48. doi:10.1016/j.chemgeo.2014.07.013
- Coward, M., Dietrich, D., 1989. an overview— Alpine tectonics. Geological Society, London, Special Publications 45.
- Deville, E., Fudral, S., Lagabriele, Y., Marthaler, M., Sartori, M., 1992. From oceanic closure to continental collision: A synthesis of the "Schistes lustrés" metamorphic complex of the Western Alps. *Geological Society of America Bulletin* 104, 127–139.
- Dowty, E., 1976. Crystal structure and crystal growth: I. The influence of internal structure on morphology. *American Mineralogist* 61, 448–459.
- Dragovic, B., Gatewood, M. P., Baxter, E. F., & Stowell, H. H. 2013. Fluid production rate during the regional metamorphism of a pelitic schist. *Contributions to Mineralogy and Petrology*, 173(11), 96.
- Dubacq, B., Bickle, M. J. & Evans, K. A., 2013. An activity model for phase equilibria in the H<sub>2</sub>O-CO<sub>2</sub>-NaCl system. *Geochimica et Cosmochimica Acta* 110, 229 - 252
- Dubacq, B., Plunder, A., 2018. Controls on Trace Element Distribution in Oxides and Silicates. *Journal of Petrology* 59, 233–256. doi:10.1093/petrology/egy027
- Dubacq, B., Vidal, O., De Andrade, V., 2010. Dehydration of dioctahedral aluminous phyllosilicates: thermodynamic modelling and implications for thermobarometric estimates. *Contributions to Mineralogy and Petrology* 159, 159–174. doi:10.1007/s00410-009-0421-6
- Epstein, G.S., Bebout, G.E., Angiboust, S., Agard, P., 2019. Scales of Fluid-Rock Interaction and Carbon Mobility in the Deeply Underplated and HP-Metamorphosed Schistes Lustrés, Western Alps. *Lithos* 105229. doi:10.1016/j.lithos.2019.105229
- Faccenda, M., 2014. Water in the slab: A trilogy. *Tectonophysics* 614, 1–30. doi:10.1016/j.tecto.2013.12.020
- Fagereng, Å., Remitti, F., Sibson, R.H., 2011. Incrementally developed slickenfibers — Geological record of repeating low stress-drop seismic events? *Tectonophysics* 510, 381–386. doi:10.1016/j.tecto.2011.08.015
- Fisher, D.M., Brantley, S.L., 2014. The role of silica redistribution in the evolution of slip instabilities along subduction interfaces: Constraints from the Kodiak accretionary complex, Alaska. *Journal of Structural Geology* 69, 395–414. doi:10.1016/j.jsg.2014.03.010
- Fornash, K.F., Whitney, D.L., Seaton, N.C.A., 2019. Lawsonite composition and zoning as an archive of metamorphic processes in subduction zones. *Geosphere*. doi:10.1130/GES01455.1
- Ganzhorn, A. C., Pilorgé, H., & Reynard, B., 2019. Porosity of metamorphic rocks and fluid migration within subduction interfaces. *Earth and Planetary Science Letters*, 522, 107-117.

- Goffe, B., Chopin, C., 1986. High-pressure metamorphism in the Western Alps: zoneography of metapelites, chronology and consequences. *Schweizerische mineralogische und petrographische Mitteilungen*, 66(1-2), 41-52.
- Goffé, B., Velde, B., 1984. Contrasted metamorphic evolutions in thrust cover units of the Briançonnais zone (French Alps): a model for the conservation of HP-LT metamorphic mineral assemblages. *Earth and Planetary Science Letters* 68, 351–360.
- Gorman, P.J., Kerrick, D.M., Connolly, J.A.D., 2006. Modeling open system metamorphic decarbonation of subducting slabs: Metamorphic decarbonation. *Geochemistry, Geophysics, Geosystems* 7, n/a-n/a. doi:10.1029/2005GC001125
- Hamelin, C., Brady, J.B., Cheney, J.T., Schumacher, J.C., Able, L.M., Sperry, A.J., 2018. Pseudomorphs after Lawsonite from Syros, Greece. *Journal of Petrology* 59, 2353–2384. doi:10.1093/petrology/egy099
- Handy, M.R., Schmid, S., Bousquet, R., Kissling, E., Bernoulli, D., 2010. Reconciling plate-tectonic reconstructions of Alpine Tethys with the geological–geophysical record of spreading and subduction in the Alps. *Earth-Science Reviews* 102, 121–158. doi:10.1016/j.earscirev.2010.06.002
- Henry, C., Burkhard, M., Goffe, B., 1996. Evolution of synmetamorphic veins and their wallrocks through a Western Alps transect: no evidence for large-scale fluid flow. Stable isotope, major- and trace-element systematics. *Chemical Geology* 127, 81–109.
- Holland, T., Baker, J., & Powell, R., 1998. Mixing properties and activity-composition relationships of chlorites in the system MgO-FeO-Al<sub>2</sub>O<sub>3</sub>-SiO<sub>2</sub>-H<sub>2</sub>O. *European Journal of Mineralogy*, 395-406.
- Holland, T.J.B., Powell, R., 1998. An internally consistent thermodynamic data set for phases of petrological interest: An internally consistent thermodynamic data set. *Journal of Metamorphic Geology* 16, 309–343. doi:10.1111/j.1525-1314.1998.00140.x
- Jaeckel, K., Bebout, G.E., Angiboust, S., 2018. Deformation-enhanced fluid and mass transfer along Western and Central Alps paleo-subduction interfaces: Significance for carbon cycling models. *Geosphere* 14, 2355–2375. doi:10.1130/GES01587.1
- Kelemen, P.B., Manning, C.E., 2015. Reevaluating carbon fluxes in subduction zones, what goes down, mostly comes up. *PNAS* 112, E4007–E4006. doi:10.1073/pnas.1507889112
- Kerrick, D.M., Connolly, J.A.D., 2001. Metamorphic devolatilization of subducted marine sediments and the transport of volatiles into the Earth's mantle. *Nature* 411, 293–296.
- Lagabriele, Y., Brovarone, A. V., & Ildefonse, B., 2015. Fossil oceanic core complexes recognized in the blueschist metaophiolites of Western Alps and Corsica. *Earth-Science Reviews*, 141, 1-26.
- Lagabriele, Y., Cannat, M., 1990. Alpine Jurassic ophiolites resemble the modern central Atlantic basement. *Geology* 18, 319–322.
- Lagabriele, Y., Lemoine, M., 1997. Alpine, Corsican and Apennine ophiolites: the slow-spreading ridge model. *Comptes Rendus de l'Académie des Sciences-Series IIA-Earth and Planetary Science* 325, 909–920.
- Lagabriele, Y., Polino, R., 1985. Origine volcano-détritique de certaines prasinites des Schistes lustrés du Queyras (France): arguments texturaux et géochimiques. *Bulletin de la Société Géologique de France* 461–471.
- Lapen, T.J., Johnson, C.M., Baumgartner, L.P., Mahlen, N.J., Beard, B.L., Amato, J.M., 2003. Burial rates during prograde metamorphism of an ultra-high-pressure terrane: an example from Lago di Cignana,

- western Alps, Italy. *Earth and Planetary Science Letters* 215, 57–72. doi:10.1016/S0012-821X(03)00455-2
- Le Pichon, X., Bergerat, F., Roulet, M.-J., 1988. Plate kinematics and tectonics leading to the Alpine belt formation; a new analysis. *Geological Society of America Special Papers* 218, 111–132.
- Lemoine, M., Bas, T., Arnaud-Vanneau, A., Arnaud, H., Dumont, T., Gidon, M., Bourbon, M., de Graciansky, P.-C., Rudkiewicz, J.-L., Megard-Galli, J., others, 1986. The continental margin of the Mesozoic Tethys in the Western Alps. *Marine and petroleum geology* 3, 179–199.
- Locatelli, M., Verlaquet, A., Agard, P., Federico, L., Angiboust, S., 2018. Intermediate-depth brecciation along the subduction plate interface (Monviso eclogite, W. Alps). *Lithos* 320–321, 378–402. doi:10.1016/j.lithos.2018.09.028
- Martin, L.A.J., Wood, B.J., Turner, S., Rushmer, T., 2011. Experimental Measurements of Trace Element Partitioning Between Lawsonite, Zoisite and Fluid and their Implication for the Composition of Arc Magmas. *Journal of Petrology* 52, 1049–1075. doi:10.1093/petrology/egr018
- Mevel, C., Kienast, J.R., 1980. Chromian jadeite, phengite, pumpellyite, and lawsonite in a high-pressure metamorphosed gabbro from the French Alps. *Mineralogical Magazine* 43, 979–984.
- Nitsch, K.-H., 1972. Das P-T-X<sub>CO2</sub> Stabilitätsfeld von Lawsonit. *Contributions to Mineralogy and Petrology* 34, 116–134.
- Oliver, N.H.S., Bons, P.D., 2001. Mechanisms of fluid flow and fluid-rock interaction in fossil metamorphic hydrothermal systems inferred from vein-wall rock patterns, geometry and microstructure. *Geofluids* 1, 137–162. doi:10.1046/j.1468-8123.2001.00013.x
- Osei Tutu, A., Sobolev, S.V., Steinberger, P., Popov, A.A., Rogozhina, I., 2018. Evaluating the Influence of Plate Boundary Friction and Mantle Viscosity on Plate Velocities: Plate boundary effect on plate motion. *Geochem. Geophys. Geosyst.* 19, 642–666. doi:10.1002/2017gc007112
- Pattison, D.R.M., De Capitani, C., Gaillardes, F., 2011. Petrological consequences of variations in metamorphic reaction affinity: Petrological consequences of variations in metamorphic reaction affinity. *Journal of Metamorphic Geology* 29, 953–977. doi:10.1111/j.1525-1314.2011.00950.x
- Piccoli, F., Vitale Brovarone, A., Beyssac, O., Martinez, I., Ague, J.J., Chaduteau, C., 2016. Carbonation by fluid–rock interaction at high-pressure conditions: Implications for carbon cycling in subduction zones. *Earth and Planetary Science Letters* 445, 146–159. doi:10.1016/j.epsl.2016.03.045
- Plank, T., Langmuir, C.H., 1998. The chemical composition of subducting sediment and its consequences for the crust and mantle. *Chemical Geology* 145, 325–394.
- Plank, T., Manning, C.E., 2019. Subducting carbon. *Nature* 574, 343–352. doi:10.1038/s41586-019-1643-z
- Plunder, A., Agard, P., Chopin, C., Okay, A.I., 2013. Geodynamics of the Tavşanlı zone, western Turkey: Insights into subduction/obduction processes. *Tectonophysics* 608, 884–903. doi:10.1016/j.tecto.2013.07.028
- Plunder, A., Agard, P., Dubacq, B., Chopin, C., Bellanger, M., 2012. How continuous and precise is the record of P-T paths? Insights from combined thermobarometry and thermodynamic modelling into subduction dynamics (Schistes Lustrés, W. Alps). *Journal of Metamorphic Geology* 30, 323–346. doi:10.1111/j.1525-1314.2011.00969.x

- Polino, R., 1984. Les séries océaniques du Haut val de Suse (Alpes Cottiennes): analyse des couvertures sédimentaires. *Ofioliti*, 9, 547-554.
- Pouchou, J.-L. & Pichoir, F., 1991. Quantitative Analysis of Homogeneous or Stratified Microvolumes Applying the Model 'PAP' in Electron Probe Quantitation. Springer US, Heinrich, K. F. J. & Newbury, D. E. (Eds.) 31-75
- Raimbourg, H., Famin, V., Palazzin, G., Mayoux, M., Jolivet, L., Ramboz, C., Yamaguchi, A., 2018. Fluid properties and dynamics along the seismogenic plate interface. *Geosphere*. doi:10.1130/GES01504.1
- Rea, D.K., Ruff, L.J., 1996. Composition and mass flux of sediment entering the world's subduction zones: implications for global sediment budgets, great earthquakes, and volcanism. *Earth and Planetary Science Letters* 140, 1–12.
- Rogers, G., Dragert, H., 2003. Episodic Tremor and Slip on the Cascadia subduction zone : the chatter of silent slip. *Science* 300, 1942–1943.
- Rosenbaum, G., Lister, G.S., 2005. The Western Alps from the Jurassic to Oligocene: spatio-temporal constraints and evolutionary reconstructions. *Earth-Science Reviews* 69, 281–306. doi:10.1016/j.earscirev.2004.10.001
- Saffer, D.M., Tobin, H.J., 2011. Hydrogeology and Mechanics of Subduction Zone Forearcs: Fluid Flow and Pore Pressure. *Annual Review of Earth and Planetary Sciences* 39, 157–186. doi:10.1146/annurev-earth-040610-133408
- Schmidt, M.W., Poli, S., 1998. Experimentally based water budgets for dehydrating slabs and consequences for arc magma generation. *Earth and Planetary Science Letters* 163, 361–379. doi:10.1016/S0012-821X(98)00142-3
- Schmidt, M.W., Poli, S., 1994. The stability of lawsonite and zoisite at high pressures: Experiments in CASH to 92 kbar and implications for the presence of hydrous phases in subducted lithosphere. *Earth and Planetary Science Letters* 124, 105–115. doi:10.1016/0012-821X(94)00080-8
- Sicard-Lochon, E., 1987. La lawsonite et ses pseudomorphes. Unpub. Ph-D Thesis, Claude Bernard-Lyon I.
- Skelton, A.D.L., Bickle, M.J., Graham, C.M., 1997. Fluid-flux and reaction rate from advective-diffusive carbonation of mafic sill margins in the Dalradian, southwest Scottish Highlands. *Earth and Planetary Science Letters* 145, 527–539. doi:10.1016/S0012-821X(96)00248-8
- Stewart, E.M., Ague, J.J., 2018. Infiltration-driven metamorphism, New England, USA: Regional CO<sub>2</sub> fluxes and implications for Devonian climate and extinctions. *Earth and Planetary Science Letters* 489, 123–134. doi:10.1016/j.epsl.2018.02.028
- Tricart, P., Lemoine, M., 1986. Les Schistes lustrés piémontais des Alpes Occidentales: approche stratigraphique, structurales et sédimentologique. doi:10.5169/SEALS-165835
- Tricart, P., Schwartz, S., 2006. A north-south section across the Queyras Schistes lustrés (Piedmont zone, Western Alps): Syn-collision refolding of a subduction wedge. *Eclogae Geologicae Helveticae* 99, 429–442. doi:10.1007/s00015-006-1197-6
- Tsujimori, T., Ernst, W.G., 2014. Lawsonite blueschists and lawsonite eclogites as proxies for palaeo-subduction zone processes: a review. *Journal of Metamorphic Geology* 32, 437–454. doi:10.1111/jmg.12057
- Ueno, T., 1999. REE-bearing sector-zoned lawsonite in the Sanbagawa pelitic schists of the eastern Kii Peninsula, central Japan. *European Journal of Mineralogy* 11, 993–998.

- van Keken, P.E., Hacker, B.R., Syracuse, E.M., Abers, G.A., 2011. Subduction factory: 4. Depth-dependent flux of H<sub>2</sub>O from subducting slabs worldwide. *Journal of Geophysical Research* 116. doi:10.1029/2010JB007922
- Verlaguet, A., Brunet, F., Goffé, B., Menut, D., Findling, N., Poinssot, C., Huet, B., 2016. Selective transfer of Li-Al-rich phyllosilicate to metamorphic veins (Western Alps): Laser Induced Breakdown Spectroscopy (LIBS) compositional profiles and microstructural characterization. *Journal of Geodynamics* 101, 51–72. doi:10.1016/j.jog.2016.05.011
- Verlaguet, A., Goffé, B., Brunet, F., Poinssot, C., Vidal, O., Findling, N., Menut, D., 2011. Metamorphic veining and mass transfer in a chemically closed system: a case study in Alpine metabauxites (western Vanoise). *Journal of Metamorphic Geology* 29, 275–300. doi:10.1111/j.1525-1314.2010.00918.x
- Vidal, O., Dubacq, B., 2009. Thermodynamic modelling of clay dehydration, stability and compositional evolution with temperature, pressure and H<sub>2</sub>O activity. *Geochimica et Cosmochimica Acta* 73, 6544–6564. doi:10.1016/j.gca.2009.07.035
- Viete, D. R., Hacker, B. R., Allen, M. B., Seward, G. G., Tobin, M. J., Kelley, C. S., Duckworth, A. R., 2018. Metamorphic records of multiple seismic cycles during subduction. *Science advances*, 4 (3), eaaq0234.
- Vitale Brovarone, A., Alard, O., Beyssac, O., Martin, L., Picatto, M., 2014. Lawsonite metasomatism and trace element recycling in subduction zones. *Journal of Metamorphic Geology* 32, 489–514. doi:10.1111/jmg.12074
- Vitale Brovarone, A., Beyssac, O., 2014. Lawsonite metasomatism: A new route for water to the deep Earth. *Earth and Planetary Science Letters* 393, 275–284. doi:10.1016/j.epsl.2014.03.001
- Wigley, M., Dubacq, B., Kampman, N., Bickle, M., 2013. Controls of sluggish, CO<sub>2</sub>-promoted, hematite and K-feldspar dissolution kinetics in sandstones. *Earth and Planetary Science Letters* 362, 76–87. doi:10.1016/j.epsl.2012.11.045
- Zack, T., John, T., 2007. An evaluation of reactive fluid flow and trace element mobility in subducting slabs. *Chemical Geology* 239, 199–216. doi:10.1016/j.chemgeo.2006.10.020

## FIGURES CAPTIONS

### Figure 1: Geological setting

A) Schematic representation of the Schistes Lustrés paleoaccretionary prism in the Alpine subduction zone (modified after Audet and Bürgmann, 2014). The three main units of the Schistes Lustrés are represented in yellow (upper unit, LPU), orange (median unit, LPM) and red (lower unit, LPL).



Liberation of fluids at the base of the seismogenic portion is conceptually represented by blue arrows.

Potential swarms of slow seismic events and/or Episodic Tremors and Slip (ETS) events are represented by white stars. B) Simplified geological map of the Cottian Alps (modified after Beyssac et al., 2002) illustrating the extent of the three Schistes Lustrés units and the sampling areas (stars) located along the Stradda del Assietta transect. The top-left inset shows the extent of the Schistes Lustrés units in the western Alps and locate the Cottian Alps. GP: Grand Paradis; FH: Flysch à Helminthoïdes; SL: Schistes Lustrés; DM: Dora Maira; PF: Penninic Front; ECM: external crystalline massifs; ICM: internal crystalline massifs. C) Schematic cross-section of the studied transect and eastward-increasing gradient of peak metamorphic conditions (modified after Agard et al., 2001a). D) Compilation of thermobarometric estimates on several Alpine units (CH: Chenaillet ophiolite, Mevel and Kienast., 1980; BR: Briançonnais, Geffroy, 1984; 1 to 5: Schistes Lustrés units, Agard et al., 2001a; MV: Mont Viso, Locatelli et al., 2018 and DM: Dora Maira, Chopin et al., 1991). Sample locations are reported on the geological map (B) and on the cross-section (C).

**Figure 2: Distribution of metasediments in the upper unit of the Schistes Lustrés complex**

A) Field photographs of the rock types (carbonate content increases from types 1 to 5). B) Average lawsonite content in each rock type. Calcschists (types 2 to 4) are the lithologies where lawsonite is clearly predominant. Mg-Fe-carpholite is found in lithology 1 only. Associated schematic logs illustrate the proportions of metasediment types. C) Rock types distribution along the path between



Fraiteve and the Assietta pass (along the path of Fig. 1b), presented on a simplified cross-section (topography not to scale). Colours as on A) and B). Calcschists are dominant overall and lawsonite is found all across the section apart from the vicinity of Testa dell'Assietta where it is in minor proportions.

**Figure 3: Structural framework and field observations on Monte Triplex**

A) Schematic representation of the Monte Triplex area (red dot on Fig. 2c). Sample locations are shown with circles. The main structural features corresponding to exhumation phases D2 and D3 (see text) are underlined. B) Photography of a Monte Triplex outcrop where the east-vergent D2 ductile phase and west-vergent D3 brittle phase are best shown. C) Photography of a typical outcrop observed in lithology 3 (calcschists) and corresponding interpretation (D). Structural features are shown for D2 (light black lines) and D3 (large grey lines). Carbonate-rich layers are represented in light brown and lawsonite-bearing veins are represented in cream colour. E) Typical alternations of folded pelite-rich and carbonate-rich layers (lithology 3). Lawsonite (Lws) is ubiquitous in pelitic layers. The black-lined shape represents the location of the hand specimen presented on figure 4. F) Lawsonite-bearing vein where host-rock inclusions of both carbonate-rich and pelite-rich layers are embedded in quartz-rich veins (lithology 2).

**Figure 4: Lawsonite in calcschists: LwsA (lithology type 3)**

A) Photography of a Monte Triplex sample (lithologies 2, 3, with fine alternations of carbonate-rich and pelite-rich layers) shown on figure 3e. Contacts between layers are magnified on C and D. LwsA crystals appear very dark due to inclusions of organic matter, easily confounded with the similarly black schistose matrix. Ankerite (Ank) is mostly found in the pelitic layers and at the lithological interfaces with the carbonate-rich layers. B) Interpretation of the same sample where LwsA crystals are represented as black prisms and ankerite in dark brown, highlighting the close association between the two minerals at the interface between pelitic and carbonate-rich layers. C) LwsA crystals in a pelitic layer with diffuse ankerite, contrasting with D) where ankerite forms well-defined horizons near lithological interface. E), F) and G) thin section micrographs showing examples of large LwsA black prisms (up to 5 mm in this sample) associated with quartz and ankerite in pelitic layers. Hourglass zonations are highlighted by colour variations and by inclusion trails of organic matter. Pale, inclusion-free lawsonite overgrows zoned, boudinaged and fractured lawsonite cores, sometimes leading to amalgamation of crystals. Qz: quartz; OM: organic matter.

### **Figure 5: Lawsonite in metamorphic veins: LwsB and LwsC**

A) Quartz-lawsonite-bearing vein showing ductile deformation in the pelitic schists. Quartz is associated with elongated cream-coloured LwsB crystals parallel to vein walls. B and C) Close-up views illustrating the association of LwsB and quartz. D) Inclusions of pelite-rich host-rock containing

LwsA and ankerite inside a LwsB-bearing vein. E) Small LwsB vein associated to ankerite and quartz.

F) and G) Tensile LwsC-bearing veins (mode I opening) opened at the hinge of quartz-bearing vein with ductile deformation in pelite (F) and in hinge of a LwsB vein (G). LwsC fibers are associated with elongated crystals of ankerite and quartz, all growing perpendicularly to the vein walls. Ank: ankerite; Qz: quartz.

**Figure 6: Textural observations of the LwsA-ankerite-quartz assemblage**

A) Thin-section scan of sample SL17-15A (polarized light) showing a lithological interface in rock type 3. Large zoned, deformed LwsA crystals with inclusion trails of organic matter are found in the pelitic domains together with quartz (Qz) and ankerite (Ank). Quartz veins, mainly found within pelitic domains, occasionally cross-cut carbonate domains as shown here. B) Close-up view in the carbonate-rich layer showing fine crystals of LwsA with quartz, ankerite, calcite and minor phyllosilicates. C) SEM back-scattered electron image of the carbonate layer focussing on lawsonite and ankerite included in a quartz-rich domain. D) Close-up view of the pelite-rich domain on image A (optical microscope in cross-polarised light) showing inclusion-free LwsA overgrowing organic-matter rich LwsA cores, co-crystallizing with large ankerite crystals and quartz. Phengite is present as a peak and retrograde phase. E) Lawsonite included in ankerite in the pelite-rich domain (optical microscope in cross-polarised light). F) SEM back-scattered electron image of inclusions of LwsA and quartz in a larger ankerite crystal, highlighting co-crystallization of the three minerals.

**Figure 7: Volumetric ratio of lawsonite and ankerite in LwsA, LwsB and LwsC-bearing samples.**

For LwsC veins, the ratios estimated including pseudomorphs (stars) are significantly higher than without pseudomorphs and are those considered, as LwsC crystals are highly retrogressed compared to LwsA and LwsB.

**Figure 8: Mineral composition.**

A) Composition of carbonates (ankerite Ank and calcite Calc), chlorite and phengite obtained from electron microprobe. The data of Plunder et al. (2012, from samples equilibrated over a larger range of peak conditions) are shown for comparison with grey symbols for phyllosilicates. B), C) and D) show the Sr and Ti content of LwsA, LwsB and LwsC, expressed in atom per formula unit from electron microprobe measurements. Uncertainties are about 10% of the measured value for each point.

**Figure 9: Element maps for lawsonite-ankerite-quartz assemblages.**

A) back-scattered electron image of a typical texture from carbonate-rich layers containing lawsonite (LwsA, Fig. 6b). Ca, Al and Fe maps obtained from electron microprobe illustrate the mineral associations. Calcite (Calc), paragonite (Pg) and chlorite (Chl) are seen on the edges of LwsA and ankerite (Ank), and post-date their crystallization. Both ankerite and calcite crystals are observed in inclusions within LwsA. B) back-scattered electron image and Sr and Ti maps obtained from SEM WDS in a LwsA crystal in a pelite-rich layer. The core of the crystal is Ti-rich, Sr enrichment is

observed on parts of the rim. C) back-scattered electron image and Sr and Ti maps obtained from SEM WDS, in a fragmented LwsA crystal preserved in a retrogressive calcite matrix. LwsA shows sector zoning with Ti-rich domains globally found in crystal cores and Sr-rich rims. D) back-scattered electron image and Mn map obtained from SEM WDS, in a LwsA-ankerite assemblage with iron oxides appearing as bright phases on the back-scattered electron image. The Mn map shows Mn-enriched domains in the ankerite-rich part of the sample, reflecting several stages of ankerite growth.

**Figure 10: Thermodynamic modelling of reactions and phase equilibria**

A) Pseudosection calculated in the CaFMASHC system with stoichiometric composition fixed by reaction (3) (see text). Peak conditions for each unit of the Schistes Lustrés complex are shown in circles. The appearance of lawsonite is shown with a bold blue line. A geothermal gradient of 8°C/km is used for the burial history, along which mineral mode evolutions is indicated in B). Along this gradient, reaction (3) occurs in the 170-190°C range. The volumetric fraction occupied by kaolinite and chlorite is replaced by lawsonite, and that of calcite by ankerite. C) and D) show pseudosections calculated for pelite-rich and carbonate-rich domains, respectively in the CaKFMASHC system. The composition of the system is shown on top of each pseudosection. Compositions are representative of each side of the lithological interface on figure 4a. Lawsonite iso-volume are represented by coloured lines and amounts are specified in dark blue. E) and F) show the evolution of mineral modes along a geothermal gradient of 8°C/km. Successive reactions producing lawsonite are detailed in the text. The

appearance/disappearance of major phases is outlined with grey bars. Temperature scales are similar to those of pseudosections above. Water is in excess in each pseudosection.

Phase equilibria are indicated in each field, numbers in small fields indicate:

A) (1) Chl, Kln, Cc; (2) Chl, Lws, Ank, Kln, Stlb, Arag, H<sub>2</sub>O; (3) Chl, Lws, Ank, Kln, Qz, Cc, H<sub>2</sub>O; (4) Chl, Kln, Ctd, Qz, Cc, H<sub>2</sub>O; (5) Ctd, Car, Qz, Cc, H<sub>2</sub>O; (6) Chl, Ctd, Ma, Qz, Ank, H<sub>2</sub>O; (7) Chl, Ma, Ank, Qz, H<sub>2</sub>O; (8) Chl, An, Qz, Cc, CO<sub>2</sub>, H<sub>2</sub>O; (9) Chl, Ank, Qz, CO<sub>2</sub>, H<sub>2</sub>O; (10) Ank, An, Qz, H<sub>2</sub>O; (11) Chl, Ank, Ma, Zo, Qz, H<sub>2</sub>O; (12) Ank, Ma, Zo, Qz, H<sub>2</sub>O.

C) (1) Chl, Kln, Cc, Phg, Ank, Qz, Stlp; (2) Chl, Ank, Kln, Phg, Cc, Qz; (3) Chl, Lws, Ank, Kln, Qz, Arag, Phg, Stlb; (4) Phg, Ank, Lws, Kln, Qz, Arag, Stlp, Mstl; (5) Phg, Ank, Lws, Kln, Qz, Stlb, Stlp, Mstl; (6) Phg, Ank, Chl, Lws, Kln, Qz, Cc, H<sub>2</sub>O; (7) Phg, Car, Ank, Lws, Kln, Qz, Stlp, H<sub>2</sub>O; (8) Phg, Ank, Chl, Kln, Qz, Cc, H<sub>2</sub>O; (9) Phg, Ctd, Ank, Chl, Kln, Qz, Cc, H<sub>2</sub>O; (10) Phg, Ctd, Car, Ank, Kln, Qz, Cc, H<sub>2</sub>O; (11) Phg, Ctd, Ank, Car, Prl, Qz, Cc, H<sub>2</sub>O; (12) Phg, Chl, Ank, Ma, Wrk, Qz, H<sub>2</sub>O; (13) Phg, Ctd, Ank, Chl, Ma, Qz, Cc, H<sub>2</sub>O; (14) Phg, Ctd, Car, Ank, Lws, Ma, Qz, H<sub>2</sub>O; (15) Phg, Ctd, Car, Ank, Lws, Prl, Qz, H<sub>2</sub>O.

D) (1) Phg, Ank, Chl, Kln, Qz, Stlb, Cc; (2) Phg, Ank, Chl, Lws, Kln, Qz, Arag, Stlp; (3) Phg, Ank, Chl, Lws, Kln, Qz, Cc, H<sub>2</sub>O; (4) Phg, Ctd, Ank, Chl, Kln, Qz, Cc, H<sub>2</sub>O; (5) Phg, Ank, Chl, Qz, Wrk,

Cc, H<sub>2</sub>O; (6) Phg, Ctd, Ank, Chl, Prl, Qz, Cc, H<sub>2</sub>O; (7) Phg, Ank, Chl, Zo, Ma, Qz, Cc, H<sub>2</sub>O; (8) Phg, Ank, Chl, Zo, Qz, Cc, H<sub>2</sub>O; (9) Phg, Ank, Lws, Qz, Arag, Act, Stlp, Mstl.

(Ank = ankerite; Act = actinote; Arag = aragonite; Car = carpholite; Cc = calcite; Chl = chlorite; Ctd = chloritoid; Kln = kaolinite; Lws = lawsonite; Ma = margarite; Mstl = Magnesio-stilpnomelane; Phg = Phengite; Qz = quartz; Stlb = Stilbite; Stlp = stilpnomelane; Wrk = wairakite ; Zo = zoisite)

**Figure 11: Petrological evolution scenario at outcrop and hand specimen scale.**

A) Progressive reaction and lithological mixing along continuous ductile deformation (D2 tectonic event, see text in section 2.2) in the calcschists. B) Shows close-up views of mineralogy at stages  $t_0$  and  $t_1$ , illustrating the main reaction consuming phyllosilicates and producing lawsonite, ankerite, quartz and water (reaction (3)) in the pelitic and carbonate domains and at their interface. C) Outcrop-scale spatial and textural relations between lawsonite types, with close-up views on veins in D). Mineral symbols are common to all subfigures. Water transfer (blue arrows) hypothesizes formation of LwsB from fluid pathways (not necessarily of external origin). LwsC are drawn in tensile veins opening at the hinge of folds and are thought to be derived from fluids with a local origin.

**Figure 12: Implications of the petrological scenario at subduction-zone scale.**

A) Summary of the inferred metamorphic evolution of the upper unit of the Schistes Lustrés complex.

LwsA crystallizes rapidly compared to the complex vein system formed progressively over most of the prograde history in the stability field of lawsonite. The small sketches and the text on the right sum up the main information regarding lawsonite formation at three different step time reported on the P-T grid. B) Schematic model of the varying properties, in particular water retention versus production of the Schistes Lustrés units at seismogenic depths. Hypothetical fluid pathways are likely found in calcschists, which produce the most water (reaction (3)). Insert on the top right as been modified after Audet and Bürgmann, 2009 and locate the studied area at depth (LFSEs = Low-frequency earthquakes).

#### TABLE CAPTION

**Table1:** Representative analysis of each type of lawsonite encountered in the studied samples.

#### SUPPLEMENTARY MATERIALS CAPTIONS

**Sup. mat. 1:** Back-scattered electron image of ankerite (Ank) included in LwsA and closely associated with quartz (Qz) in a pelite-rich domain. Pg: paragonite.

**Sup. mat. 2:** The top image shows a compositional map of Ca obtained from SEM on a thin section (sample SL17-08D3), used to estimate the Lws/Ank ratio presented in figure 7. LwsA is represented in dark blue, ankerite in light blue and calcite in red. The two photographs below (optical microscopy)



illustrate the typical textures of lawsonite-bearing veins (LwsB and LwsC). Depending on the retrogression state, Lws/Ank might have been estimated on Lawsonite ghosts (pseudomorphs, LwsC\*) as shown for the LwsC bearing vein.

**Sup. mat. 3:** Optical microscopy (cross-polarized light) image centered on a LwsA crystal with ankerite (Ank) inclusions in a pelite-rich layer. The two chemical maps below illustrate hourglass zonation of Ti and Sr in this lawsonite crystal. Cc: calcite; Phg: phengite Qz: quartz..

**Sup. mat. 4:** Supplementary pseudosection calculated for pelite-rich composition (R11SCH, see Fig.10c) in the CaKFMASHC system. The composition of the system is shown on top of the grid. The water content has been fixed to 15wt.% to verify the saturated water state in pseudosection shown in figure 10c. The associated mineral modes are drawn below. The main lawsonite-ankerite forming reaction still occurs at 170-180°C, although the reaction is complicated by the contribution of stilbite breakdown. The mineral mode evolution remains unchanged, as well as carpholite-in and out reactions. The appearance of major phases is outlined with grey bars. All symbols and abbreviations are similar to those in figure 10.

## Highlights

- Voluminous lawsonite stable in calcschists at the base of the seismogenic zone
- Co-crystallization of lawsonite and ankerite witnesses carbon retention
- Sequential crystallization of hydrous phases constrains fluid budget and migration
- Vein-forming reactions consistent with closed-system behaviour

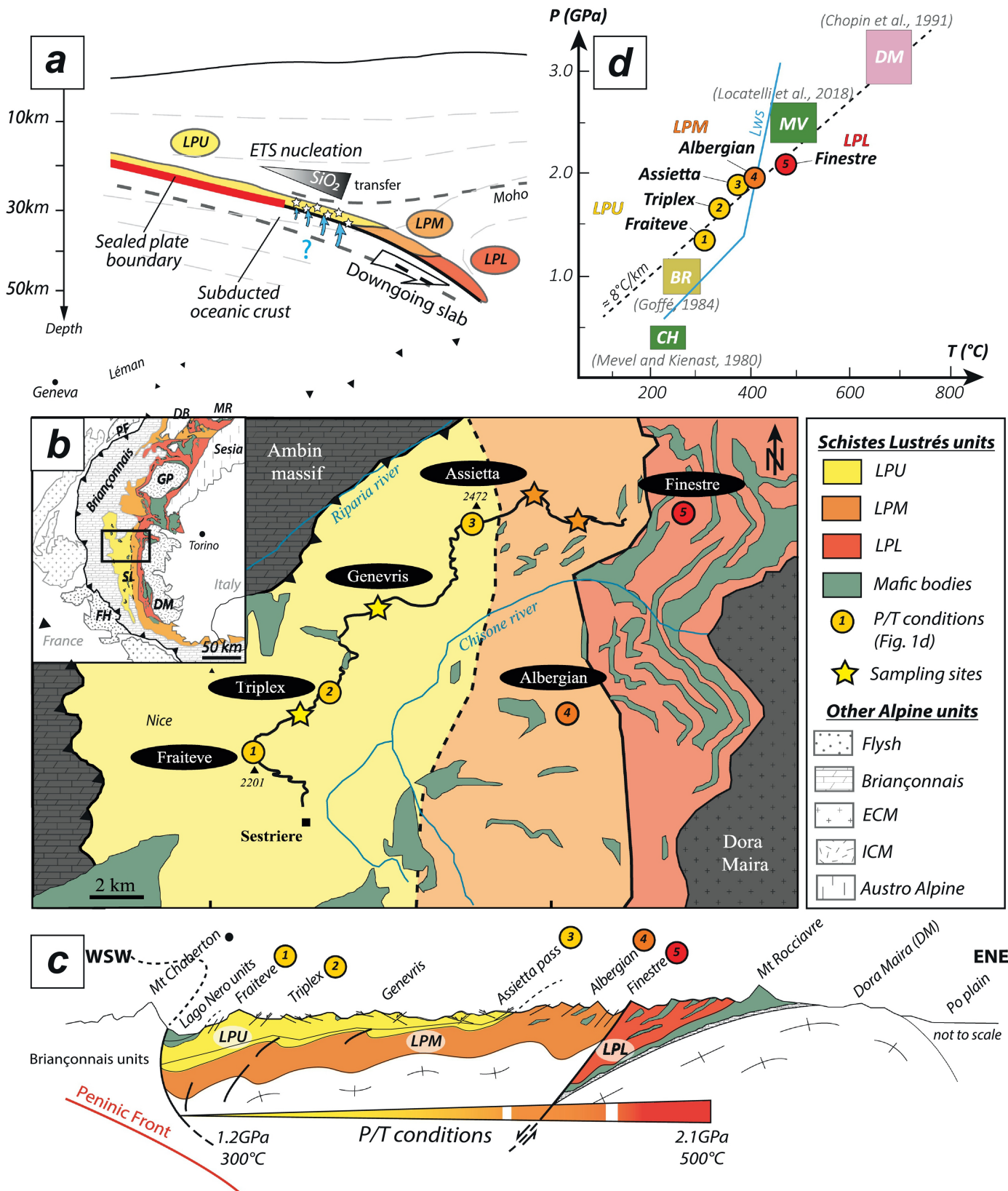


Figure 1

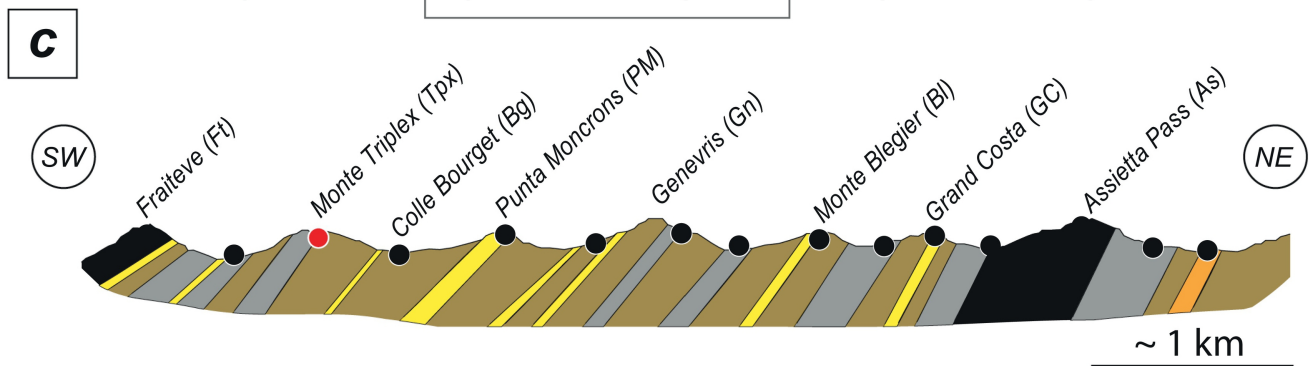
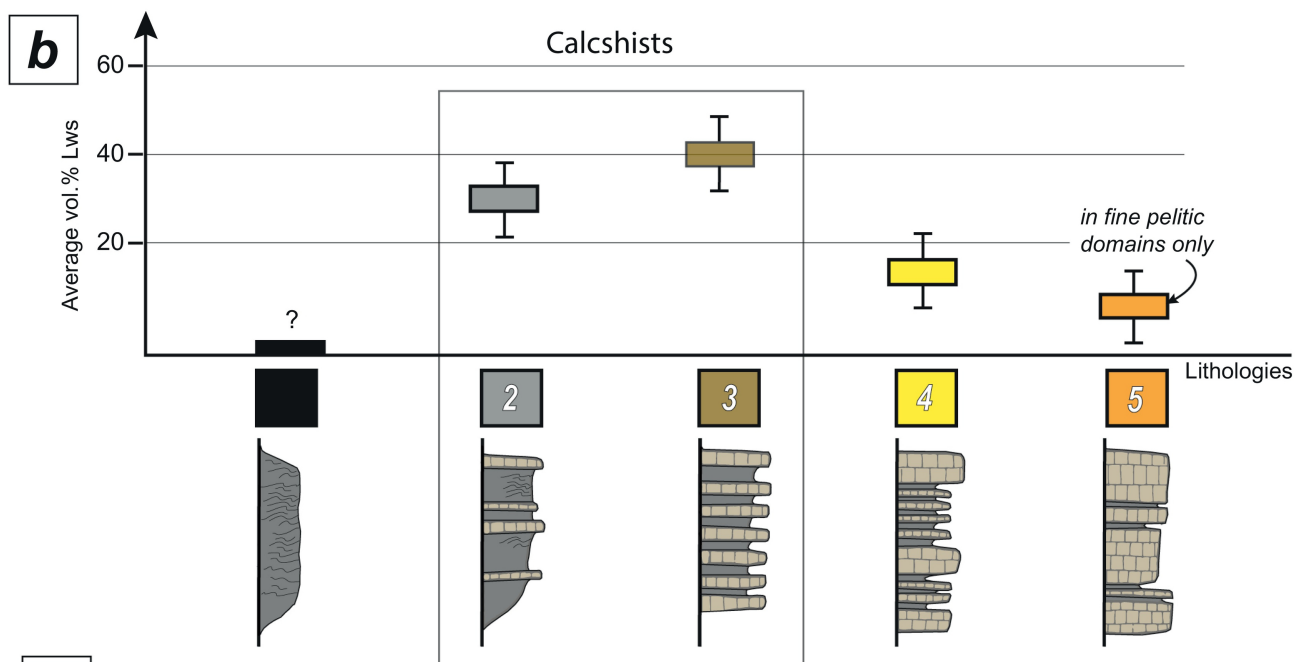
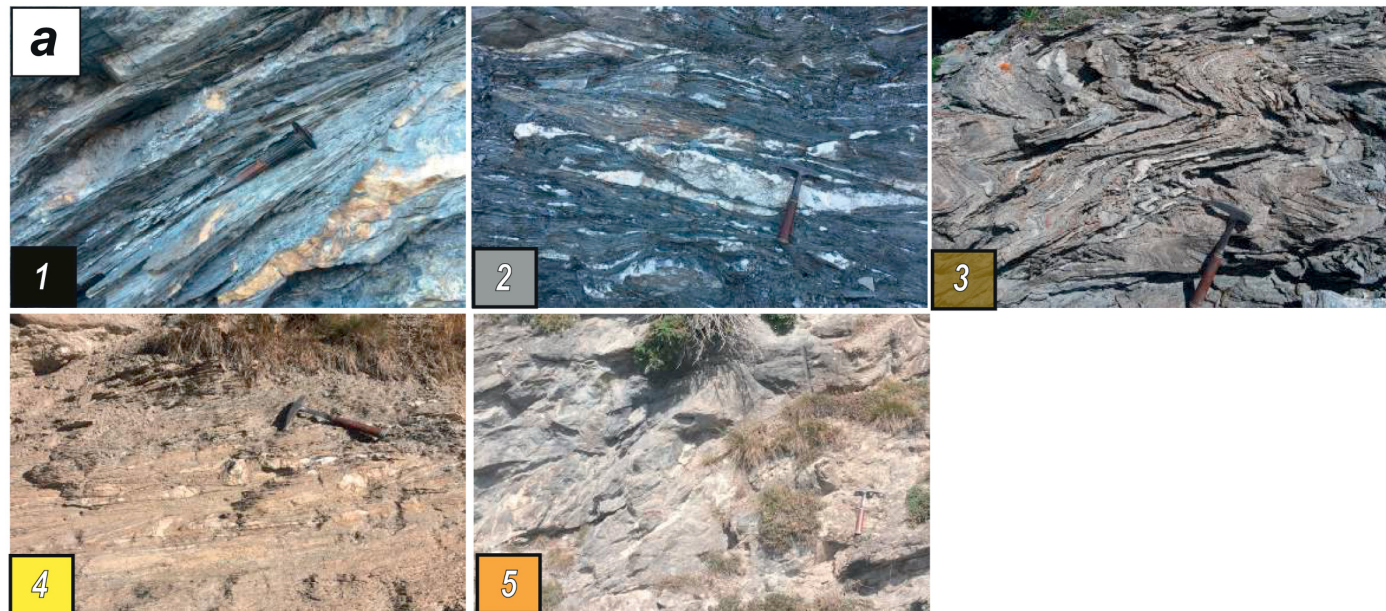


Figure 2



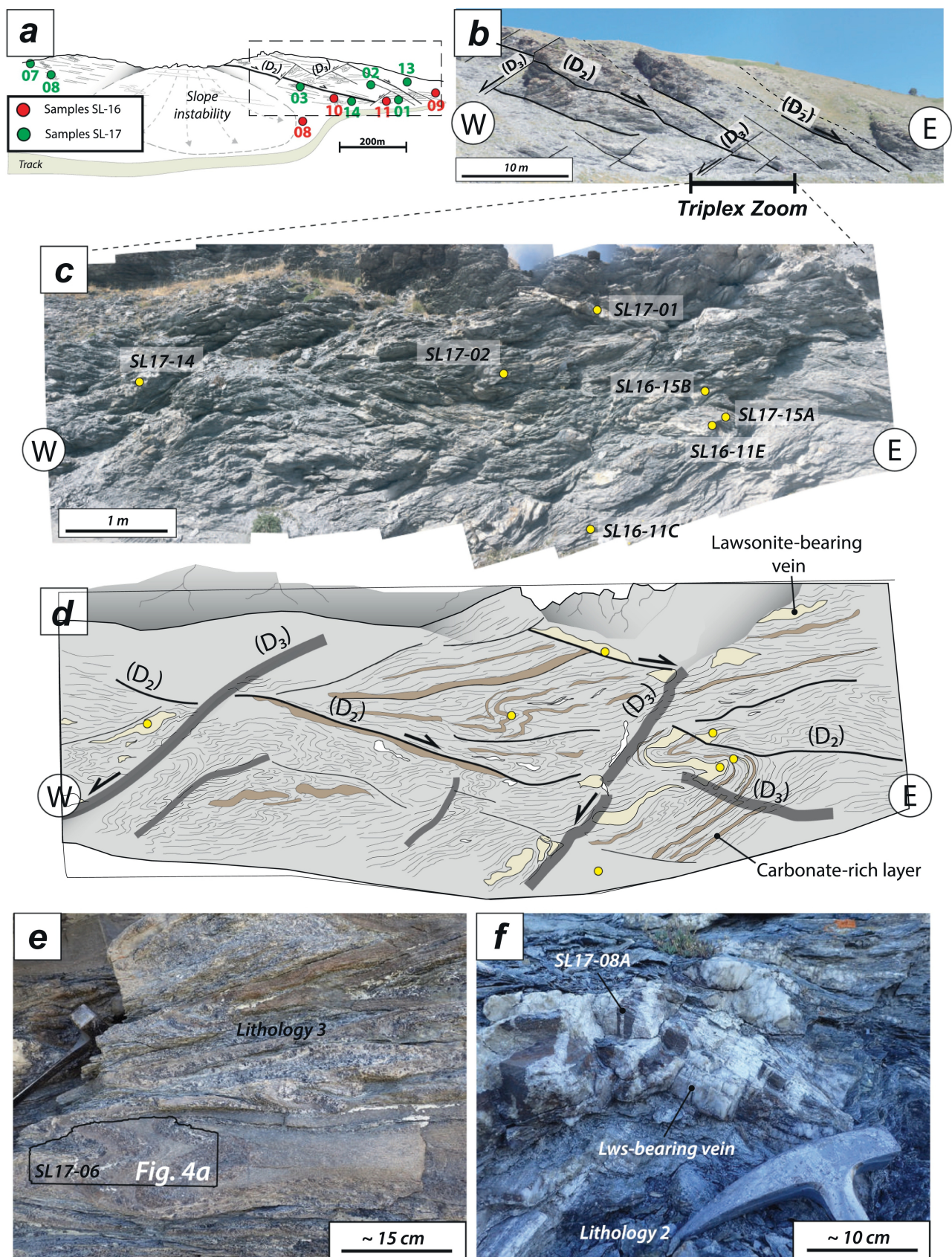


Figure 3



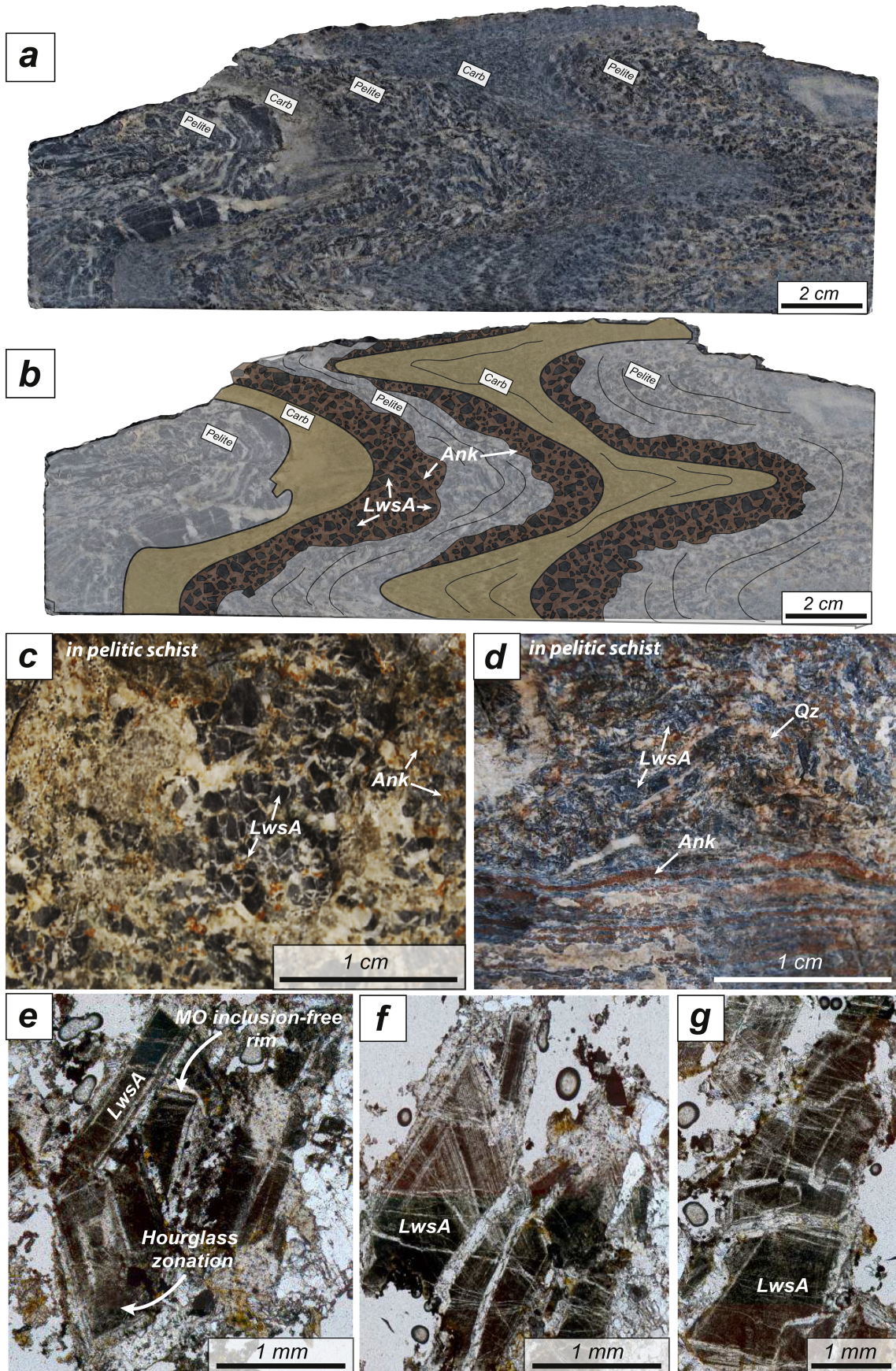


Figure 4



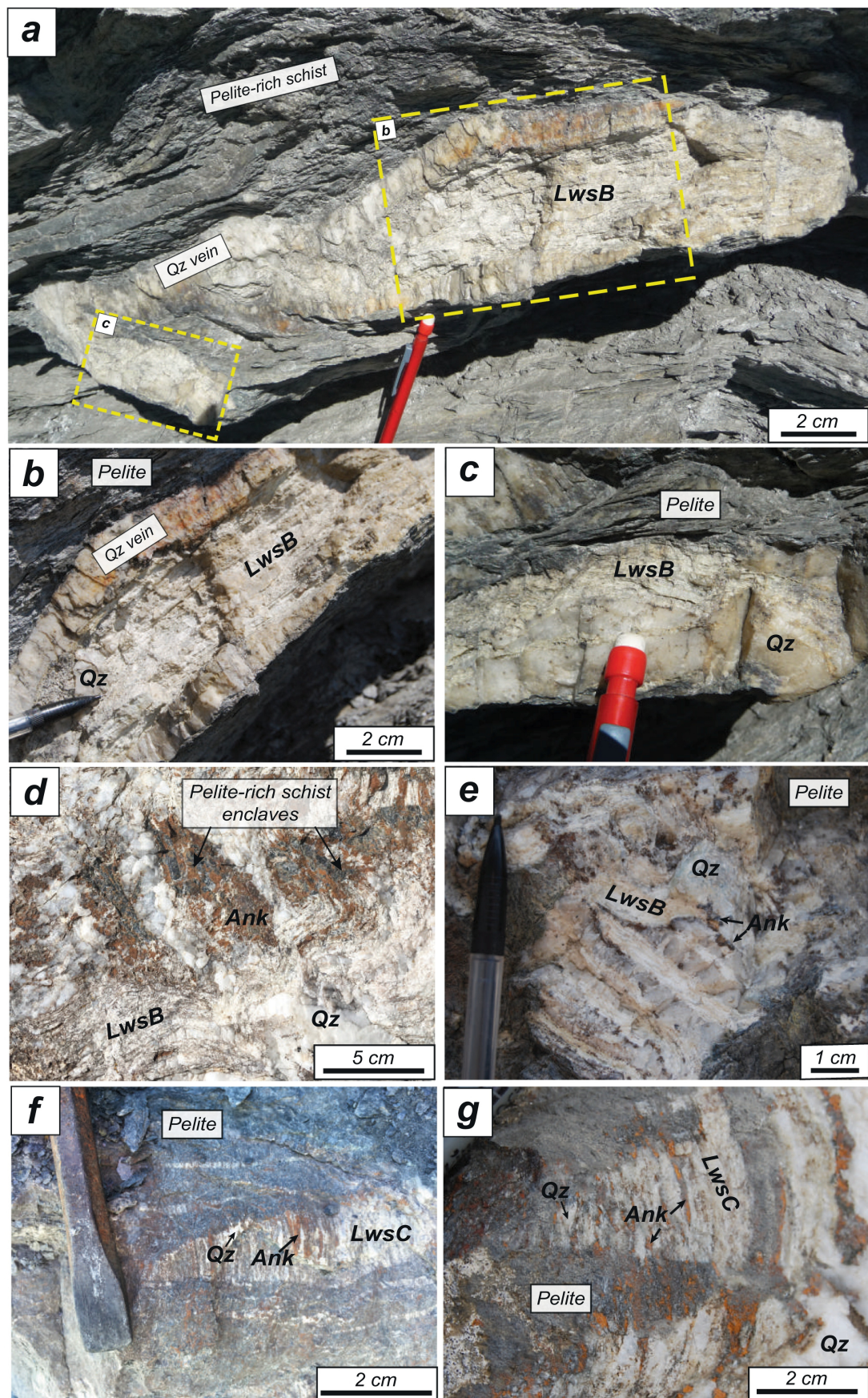


Figure 5



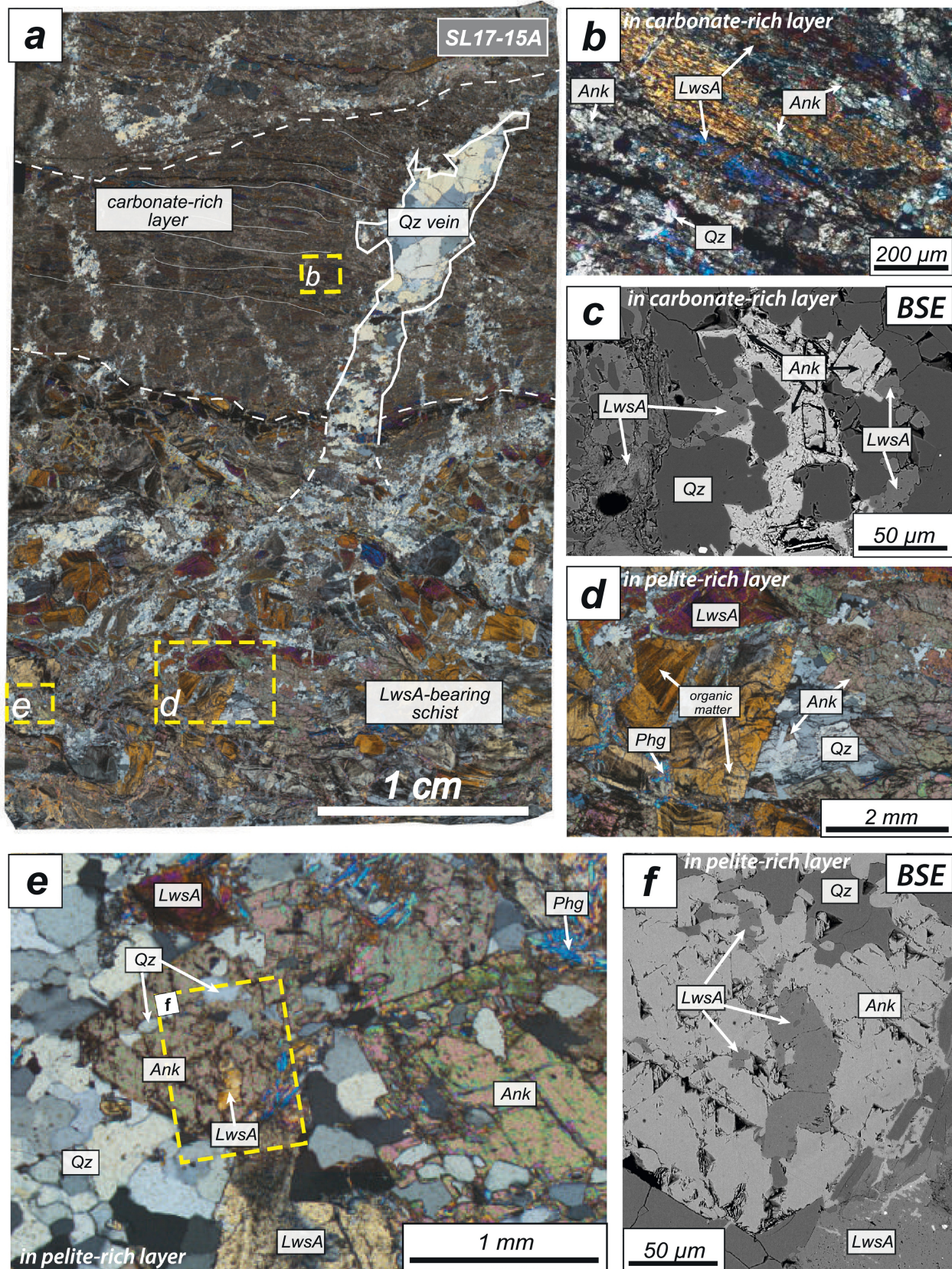


Figure 6



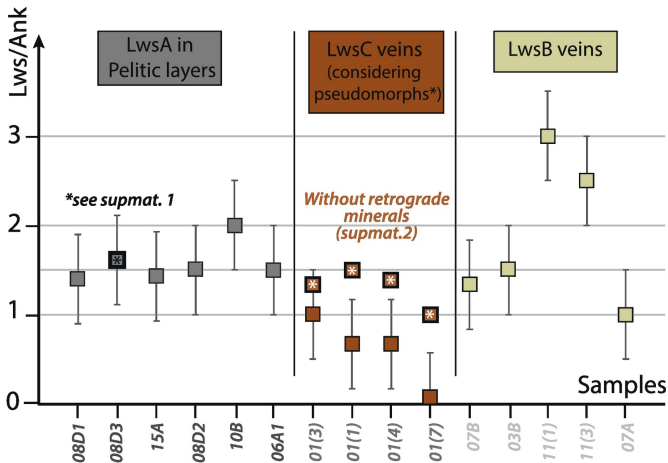


Figure 7

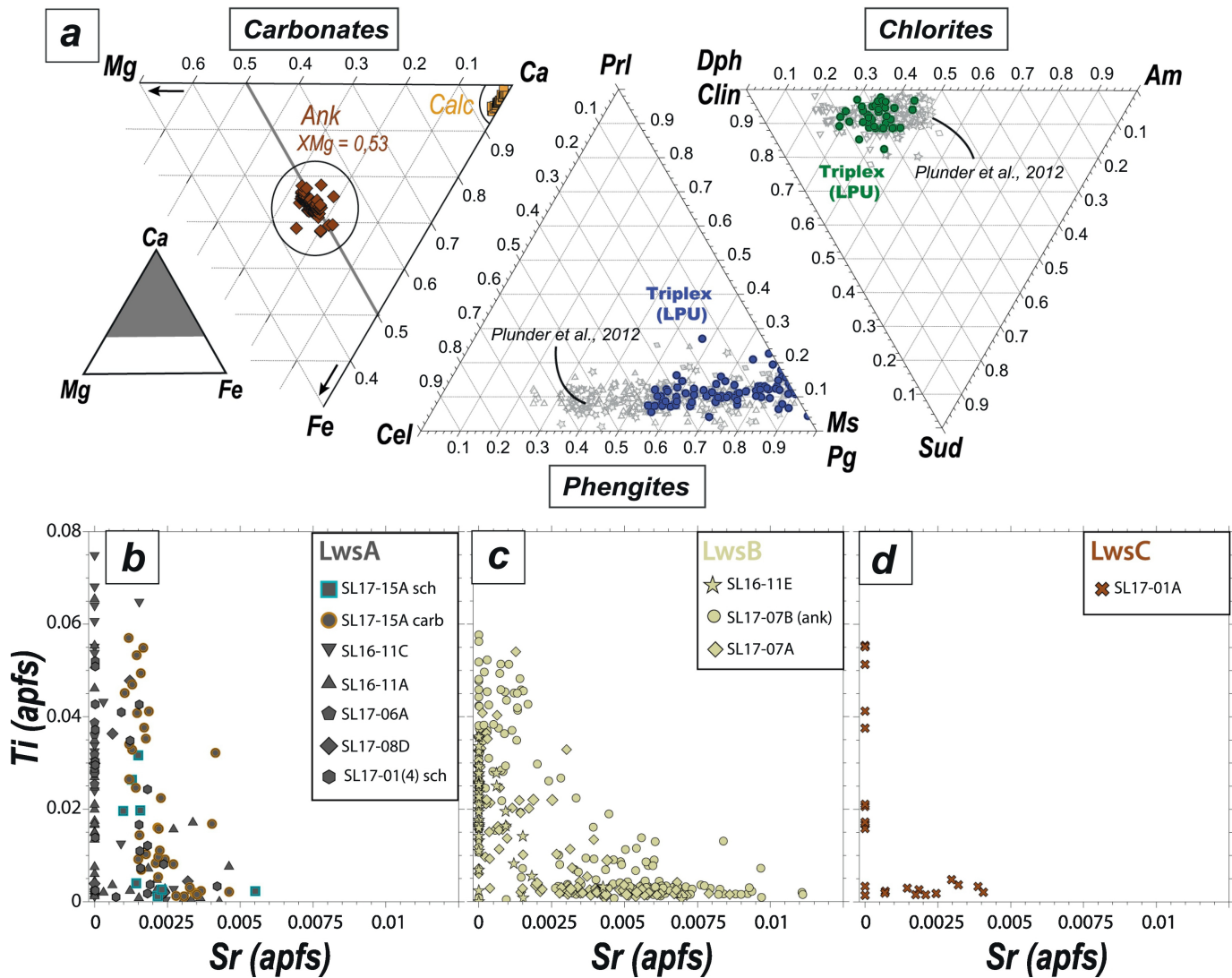


Figure 8

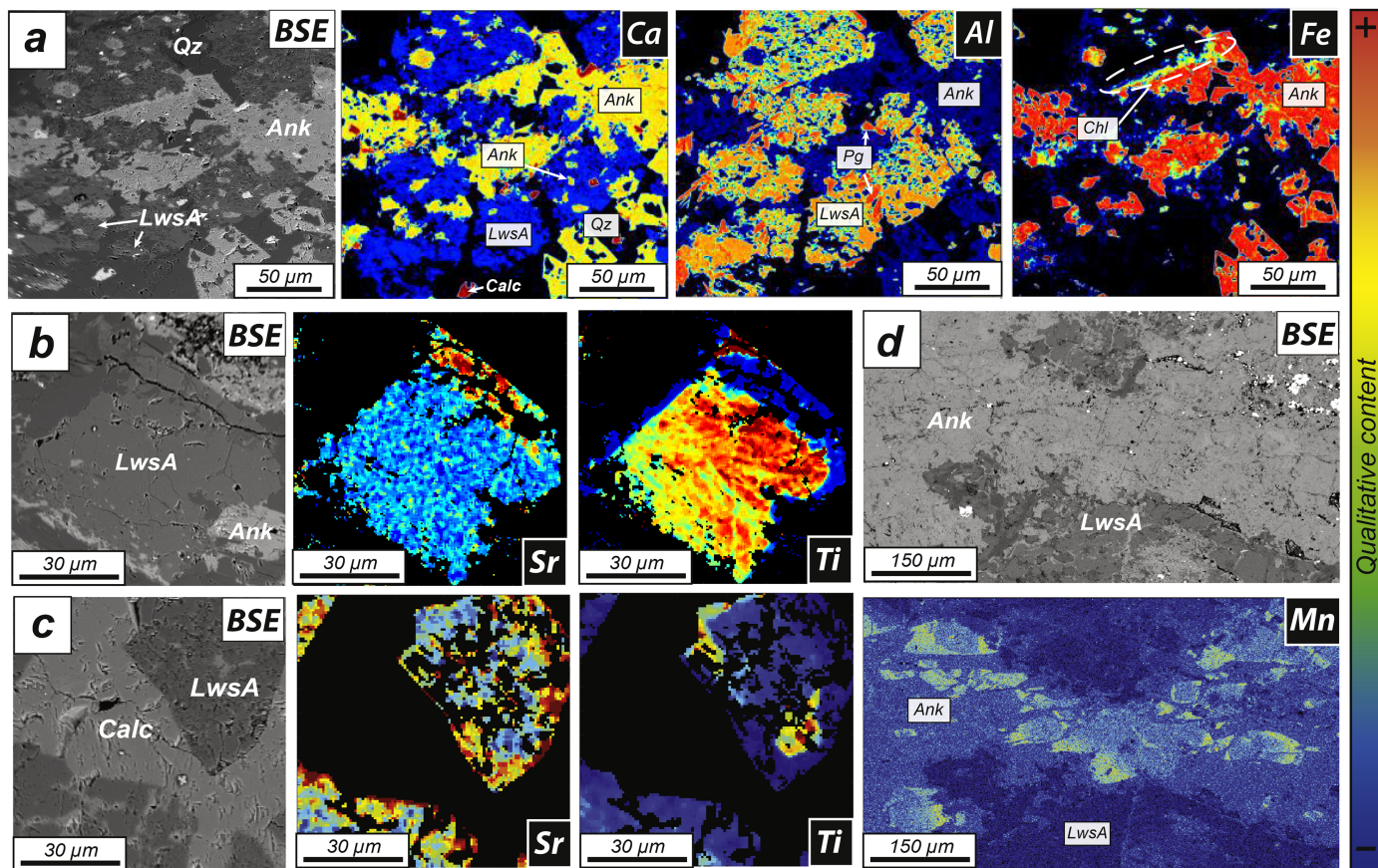
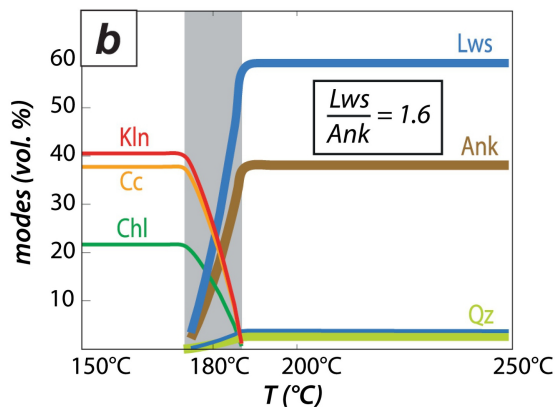


Figure 9

$$3.8 \text{ SiO}_2 \cdot 2.0 \text{ Al}_2\text{O}_3 \cdot 0.5 \text{ FeO} \cdot 0.5 \text{ MgO} \cdot 2.0 \text{ CaO} \cdot 2.0 \text{ CO}_2 \cdot 2.0 \text{ H}_2\text{O}$$


47.34 SiO<sub>2</sub> 23.24 Al<sub>2</sub>O<sub>3</sub> 5.51 FeO 3.39 MgO 13.32 CaO 1.9 K<sub>2</sub>O 10.46 CO<sub>2</sub> 8 H<sub>2</sub>O

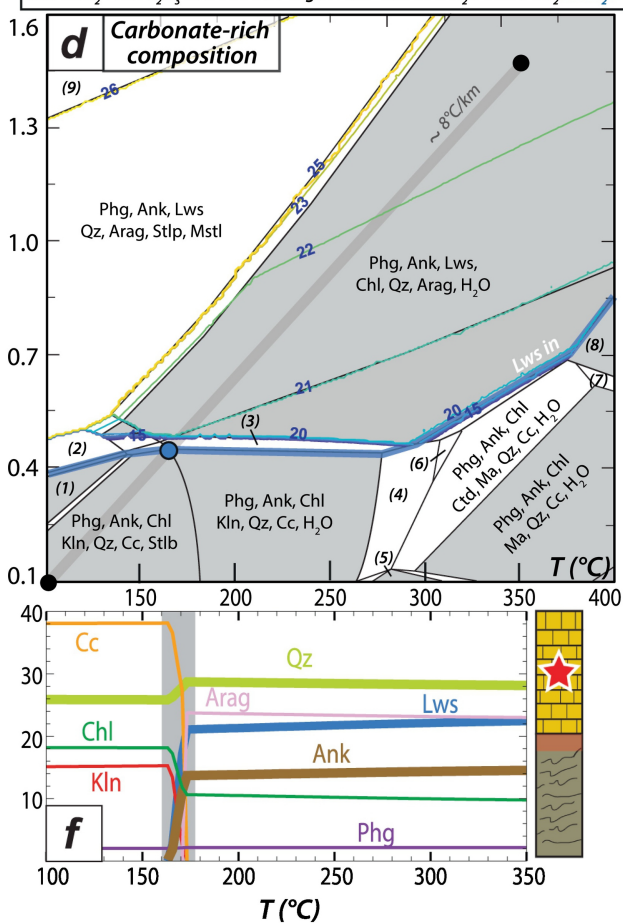
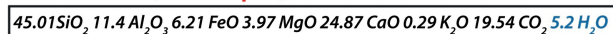


Figure 10



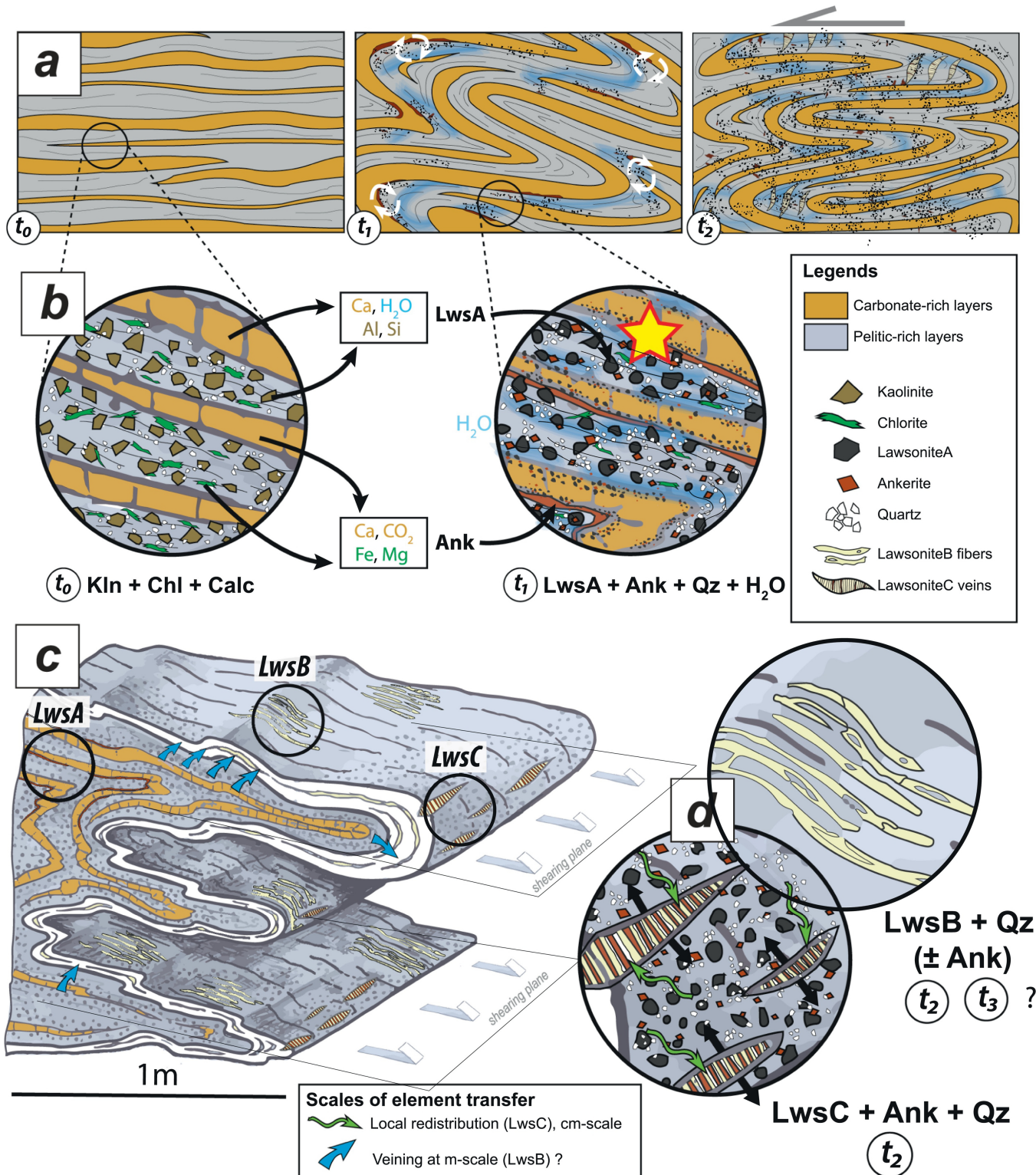


Figure 11

